

Article

Selective Calcium Removal at Near-Ambient Temperature in a Multimineral Recovery Process from Seawater Reverse Osmosis Synthetic Brine and Ex Ante Life Cycle Assessment

Raffaele Molinari ^{1,*} , Ahmet Halil Avci ¹ , Efrem Curcio ¹, David Sanchez Domene ², Carolina Villa González ², Jose Jorge Espi Gallart ² and Pietro Argurio ¹ 

¹ Department of Environmental Engineering (DIAM), University of Calabria, via P. Bucci, cubo 44/A, I-87036 Arcavacata di Rende (CS), Italy; ahmethalilavci@hotmail.com (A.H.A.); efrem.curcio@unical.it (E.C.); pietro.argurio@unical.it (P.A.)

² Eurecat, Centre Tecnològic de Catalunya, Waste, Energy and Environmental Impact, 08243 Manresa, Spain; david.sanchez@eurecat.org (D.S.D.); carolina.villa@eurecat.org (C.V.G.); josejorge.espi@eurecat.org (J.J.E.G.)

* Correspondence: raffaele.molinari@unical.it

Abstract: Potable water production from seawater generates brines that can produce stress in ecosystems, but they are also a potential source of metal and minerals. In our multi-mineral modular seawater brine mining process under development, calcium removal with minimal magnesium removal was the first stage. Even though calcium removal from reverse osmosis brine has been widely studied, there is no relevant research on its precipitation by carbonates at a near-ambient temperature (a range of 15–35 °C) and its selectivity over other minerals, as well as studies on operating conditions for selective precipitation considering the presence of antiscalants. We studied its reaction kinetics and equilibrium and conducted an ex ante life cycle assessment (LCA). The control of pH levels together with the Ostwald ripening process were very important factors to obtain a selective CaCO₃ precipitation. The first-order average kinetic constant of the precipitation at 35 °C was 0.582 ± 0.141 h⁻¹. The presence of minor ions and an antiscalant did not influence the precipitation, obtaining 85–90% on average for the %Ca²⁺ precipitation while the Mg²⁺ co-precipitation was lower than 5–7%. A lab-scale plant, tested in continuous (5 L/h synthetic brine) and in batch (15 L) modes, showed that the latter performs better and could be of interest at a larger scale. The ex ante LCA for the batch (100 L) showed that the main environmentally impactful factors were the thermostatic heating and the addition of a precipitant (Na₂CO₃), but these could be mitigated at the industrial level.

Keywords: seawater brine mining; reverse osmosis seawater brine use; selective calcium carbonate precipitation; zero liquid discharge; ex ante LCA



Citation: Molinari, R.; Avci, A.H.; Curcio, E.; Domene, D.S.; Villa González, C.; Gallart, J.J.E.; Argurio, P. Selective Calcium Removal at Near-Ambient Temperature in a Multimineral Recovery Process from Seawater Reverse Osmosis Synthetic Brine and Ex Ante Life Cycle Assessment. *Water* **2024**, *16*, 667. <https://doi.org/10.3390/w16050667>

Academic Editor: John Zhou

Received: 10 January 2024

Revised: 20 February 2024

Accepted: 22 February 2024

Published: 24 February 2024



Copyright: © 2024 by the authors. Licensee MDPI, Basel, Switzerland. This article is an open access article distributed under the terms and conditions of the Creative Commons Attribution (CC BY) license (<https://creativecommons.org/licenses/by/4.0/>).

1. Introduction

The demand for potable water for different uses, such as drinking water, industrial or agricultural processes, food processing, etc., is continuously growing, and much interest is devoted to seawater (SW) as the main water source on the planet, making up 97% of the total water [1]. The desalination of the SW can be accomplished with current commercial technologies, such as reverse osmosis (RO), multi-stage flash (MSF), multi-effect distillation (MED), mechanical vapor compression, and electrodialysis. Nowadays, RO is the most widespread technology for desalination, followed by MSF and MED [2]. The produced reject (usually named “brine”) cannot be discharged in the environment because of its deleterious impact on aquatic and terrestrial ecosystems and because a large amount of water is lost as well as valuable minerals and nutrients [3–5]. Brines are high-salinity streams that come from various processes, such as oil and gas exploration, desalination concentrate, landfill leachate, wastewaters from the coal-to-chemical process, textiles,

mining, and leather tanning [6]. Desalination concentrate from SW or brackish water by RO generates an amount of RO brine that, depending on the feed water quality, is roughly 300 to 2000 m³ for every 1000 m³ of treated water produced in a typical RO system [7]. Currently, worldwide desalination plants produce about 142,000,000 m³/day, and the produced desalination brine is estimated at 128,652,000 m³/day [8]. Because SW contains almost all the elements of the periodic table at ppm/ppb levels [9], we can estimate the amounts of metals that could be recovered from SW brines in terms of various tons per day.

In the context of the circular economy, the European Commission established a list of critical raw materials (CRMs) on the basis of their high economic importance and high supply risk [10]; thus, research activities on innovative mining and recycling processes have been encouraged accordingly. To promote multi-element recovery from SW, the European Union Horizon 2020 project “Development of radical innovations to recover minerals and metals from SW desalination brines” (<https://sea4value.eu/>, accessed on 9 January 2024) is currently running to develop highly efficient separation technologies. Many studies exist in the literature on different separation technologies for brine treatment [1,6,11,12] for the proper management of hypersaline streams to decrease the amount of dewatered brine while increasing the amount of available freshwater [3,4]. A study by Panagopoulos and Haralambous [8] showed that increasing the amount of recovered freshwater is not always cost effective. Indeed, a comparison of the strategies of minimal liquid discharge (MLD) and zero liquid discharge (ZLD) showed that, even though the total freshwater recovery from the ZLD system was 98.15% versus 84.6% from the MLD system, the energy consumption of the ZLD system was 10.43 kWh/m³, which was 1.93 times higher than the energy consumption of the MLD system (5.4 kWh/m³). So, the most useful strategy should be valued for wastewater utilization, reuse, and resource recovery. In another case, an economical evaluation based on capital expenses (CAPEX) and operating expenses (OPEX) was applied by Figueira et al. [13] in the NF pretreatment of SW brine to choose whether it would be better to place the NF before or after a Ca(II) precipitation stage, considering that Ca(II) can produce scaling in membranes. Another approach to evaluate the feasibility of a process is estimating its environmental profile by means of ex ante life cycle assessments (ex ante LCAs). Emerging technologies, such as the one presented here, often have results that are available with lab- or pilot-scale validation. In these cases, the use of an ex ante LCA as an early environmental assessment provides preliminary insights that allow us to incorporate the environmental performance as an additional factor of the development phase of technologies, thus influencing technological developments and sustainable innovations [14].

In the various methods of brine processing and re-use, a pretreatment step is a common practice for calcium removal together with magnesium or alone [15,16]. In the case of the brine pre-concentration and the subsequent extraction of valuable minerals, the removal of calcium in the upstream section is usually performed to avoid the formation of inorganic salts in the downstream sections, which may reduce the flow rate through the pipes, drop the efficiency of heat exchangers, and decrease the productivity of membrane and thermal processes [17]. The inorganic salts—properly referred to as “scaling”—are related to the precipitation of sparingly Ca-soluble salts, such as CaCO₃(s) and CaSO₄·2H₂O [18]. When brine from RO plants was tested as a source of industrial water in the copper mining industry, the removal of and reduction in the calcium and magnesium ion concentration were also required to improve the copper recovery in the flotation process [19]. Magnesium and calcium removal in sequence was also studied in the pretreatment of desalination brine before subjecting it to electrolysis [20,21]. In the concentration of SWRO brines by electrodialysis, a calcium removal of 94–96% as carbonate with simultaneous magnesium removal higher than 60% at 60 °C was obtained by Casas et al. [22]. Wang et al. [23] used a temperature between 70 and 85 °C while Molinari et al. [24] used a temperature between 60 and 70 °C for a selective calcium precipitation as carbonate, both obtaining similar performances (with the Ca²⁺ precipitation around 90% and the Mg²⁺ precipitation below 7%).

In the present work, the removal of calcium as carbonate (by minimizing Mg removal) is the first stage of RO brine processing to use it as a freshwater source and recover a set of commodity and specialty minerals and metals (Ca(II), Mg(II), B(III), Sc (III), V(V), In(III), Ga(III), Li(I), Mo(VI), and Rb(I)). The removal of calcium is performed first to mitigate the problem of inorganic scaling as previously mentioned and to minimize calcium interference in downstream separation processes [25]. However, the above-reported approaches for calcium removal as carbonate require the heating of the brine and could be energetically acceptable if the next step is the distillation of the membrane or an evaporation-based operation. Excluding these specific cases, a more sustainable approach, from an energy standpoint, is to operate at a temperature closer to an ambient one, which is the main aim of the experimental study described in this work. Usually, the brine from RO plants is discharged at a range of 15–35 °C, so an investigation into the performance of the selective separation of calcium in this temperature range is of interest. It must be pointed out that in the previous work of Molinari et al. [24], other than the higher temperature range, the hydrogen carbonate ion at a molar ratio of $\text{HCO}_3^-/\text{Ca}^{2+} = 3$ was used, and the precipitant excess can result noxious in the downstream stages. For this reason, the carbonate ion instead of the hydrogen carbonate ion has been used in this work as the precipitant source to reduce this ratio, but its different chemical behavior requires us to determine all the parameters influencing the selective precipitation. So, after a preliminary study on the theoretical thermodynamic and kinetic aspects of CaCO_3 precipitation by carbonate, various parameters are experimentally studied: (i) the sodium carbonate concentration to minimize magnesium co-precipitation; (ii) the choice of the molar ratio of $\text{CO}_3^{2-}/\text{Ca}^{2+}$ and addition mode of sodium carbonate; (iii) the temperature's effect on the CaCO_3 precipitation; (iv) an antiscalant's effect on the CaCO_3 precipitation; (v) the effect of the initial concentration of the simulated brine on the precipitation kinetics; (vi) the Ostwald ripening effect on the CaCO_3 precipitation; and (vii) the presence of minor ions in the simulated brine. Finally, the obtained results are used to design and build a lab-scale plant working in batch and in continuous modes to test the calcium precipitation and collect useful information for the up-scaling of this process. Then an estimation of the energy saved in the calcium precipitation at low versus high temperatures and an estimation of the environmental profile of the calcium precipitation by an ex ante LCA are reported.

2. Material and Methods

2.1. Reagents

Various salts were used to prepare synthetic brine solutions by dissolving them into Milli-Q water: $\text{CaCl}_2 \cdot 2\text{H}_2\text{O}$ (RCS grade, from Riedel de Haen, Seelze, Germany), $\text{MgCl}_2 \cdot 6\text{H}_2\text{O}$ (>99%, from Panreac, Darmstadt, Germany), Na_2SO_4 (ACS grade, from Sigma Aldrich, St. Louis, MA, USA), NaCl (>99%, from Sigma Aldrich), KCl (ACS grade, from Sigma Aldrich), NaHCO_3 (>99%, from Panreac), Na_2CO_3 (>99.5%, from Sigma Aldrich), Strontium chloride SrCl_2 (anhydrous $\geq 99.5\%$ (metals basis), from Alfa Aesar, Ward Hill, MA, USA), Boron standard solution for ICP (10,000 mg/L B in ammonium hydroxide solution, from VWR chemicals, Radnor, PA, USA), Rubidium standard solution for ICP (10,000 mg/L Rb in diluted nitric acid, from VWR chemicals, Radnor, PA, USA), Lithium standard solution for ICP (10,000 mg/L Li in diluted nitric acid, from VWR chemicals, Radnor, PA, USA), Indium standard solution for ICP (1000 mg/L In in diluted nitric acid, from VWR chemicals, Radnor, PA, USA), Molybdenum standard solution for ICP (10,000 mg/L Mo in ammonium hydroxide solution (max. 1%), from VWR chemicals, Radnor, PA, USA), Vanadium standard solution for ICP (1000 mg/L V in diluted nitric acid, from VWR chemicals, Radnor, PA, USA), Scandium standard solution for ICP (1000 mg/L Sc in diluted nitric acid, from VWR chemicals, Radnor, PA, USA), and Gallium standard solution for ICP (1000 mg/L Ga in diluted nitric acid, from VWR chemicals, Radnor, PA, USA). Permatreat™ PC-1020T from Nalco (Montebelluna, Italy) was used to study the antiscalant's effect.

The pH of the solutions was adjusted by addition of diluted NaOH or HCl.

The precipitation tests were performed with two SWRO synthetic brine concentrations. In the lab-scale plant (Section 4.7), whose results are of interest for the upscaling of the process, a synthetic brine with concentration double (2xSB) that of the original (SB) was used, as will be discussed in Section 4.4. So, in Table 1, the composition of the 2xSB solution, including both the concentration of the major and minor ions, is reported. However, for most parts of the preliminary experiments, the original SB (with a concentration of major ions that was half that reported in Table 1) was used. In Section 4.4, 3xSB and 4xSB brines have also been used and discussed to test the effectiveness of the antiscalant, but they were not used for the precipitation tests.

Table 1. Reagents and ions concentration (major and minor) of two-fold concentrated synthetic brine (2xSB).

Reagent	Major Ions		Reagent	Minor Ions	
	Concentration (g/L)	Concentration (mM)		Concentration (g/L)	Concentration (mM)
NaCl	96.30	1660	Sr(II)	48×10^{-3}	0.55
MgCl ₂	21.96	230	B(III)	17×10^{-3}	1.57
Na ₂ SO ₄	16.76	118	Rb(I)	0.60×10^{-3}	0.0070
CaCl ₂	4.76	43	Li(I)	0.82×10^{-3}	0.12
KCl	3.05	41	In(III)	0.125×10^{-3}	0.0011
NaHCO ₃	0.26	3.1	Mo(VI)	0.125×10^{-3}	0.0013
Na ₂ CO ₃	0.085	0.8	V(V)	0.125×10^{-3}	0.0024
/	/	/	Sc(III)	0.125×10^{-3}	0.0028
/	/	/	Ga(III)	0.125×10^{-3}	0.0018

Na₂CO₃ solutions with various concentrations (range of 0.65–2.36 M) were used as precipitant as reported in the figure's legends.

2.2. Analytical Methods

A pH meter (WTW Inolab Terminal Level 3) with a glass pH electrode SenTix 81 (WTW) was used for pH measurements.

Major ions (i.e. Ca²⁺, Mg²⁺) in the liquid samples were quantified by using a ContraAA 700 high-resolution continuum source atomic absorption spectrometer (HR-CS AAS) (Analytik Jena AG, Jena, Germany) with a high-intensity Xe short-arc lamp as continuum source, calibrated with ICP multi-element IV standard solution from Merck. Method parameters (i.e., fuel flow and burner height) were obtained by the flame automatic optimization procedure for the determination of Ca and Mg. The absorbance measurements were performed using the 422.67 nm and 285.21 nm spectral lines for the determination of Ca and Mg, respectively. The reproducibility of the determination of Ca²⁺ and Mg²⁺ concentration was within $\pm 5\%$. Liquid samples (with a volume of 25–50 μ L) were withdrawn and properly diluted with Milli-Q water to the calibration range of atomic absorption, i.e., 0–3.5 mg/L for Mg, and acidified with 1% *v/v* HCl. Since the precipitation tests were performed under agitation, the stirring was stopped for 10 min before sampling to avoid the possible withdrawal of suspended precipitate in the liquid sample.

Quantification of minor ions was carried out by means ICP-MS analyses at Eurecat (Manresa, Spain) by applying the standard methodology.

The solid precipitate samples were analyzed after acidic dissolution to determine the Ca and Mg content. For this purpose, 0.1 g of each dried precipitate sample was dissolved in 250 mL of ultrapure water by the help of 2.5 mL HCl (37%). The obtained solutions were diluted 100 times in order to fit into the calibration range and were analyzed using HR-CS

AAS ContrAA 700, thus determining the amount of Ca and Mg and calculating the Ca/Mg mass ratio in the dried precipitate.

Analytical determination via AAS concerned mainly calcium and magnesium ions which were involved in the precipitation process, while the effect of the other ions was tested by analyzing the precipitate via powder X-ray diffraction (XRD) to determine the composition and the major mineral phases of the crystalline content in the samples. The samples were homogenized and, if necessary, ground, before analysis. Analyses were carried out on a Bruker[®] D5005 X-ray diffractometer in θ - θ mode with Cu K α radiation. Repeated continuous scans were performed on rotating samples in the 2θ range 0–60° at a rate of 0.025°/18 s. Granular precipitates were also observed under a JEOL[®] JSM840 field emission scanning electron microscope with Oxford Link[®] energy dispersive system (SEM-EDS).

2.3. Methodology of the Preliminary Precipitation Tests

To collect information on some parameters involved in the precipitation reaction such as (i) molar ratio $\text{CO}_3^{2-}/\text{Ca}^{2+}$, (ii) precipitant feeding mode, (iii) temperature, (iv) antiscalant presence, and (v) feed concentration, preliminary precipitation tests were carried out by employing SB solutions (tests i–iv). Some tests using a 4x feed solution containing only Ca^{2+} and Mg^{2+} (4xCaMg), (test v_a), and a 2xSB solution (test v_b) were also performed. The temperature was always 35 °C except in some tests in which it was 15 °C or 60 °C, as reported. Below the details of the methodology used for carrying out these tests are reported.

(i) *Tests to determine the optimal $\text{CO}_3^{2-}/\text{Ca}^{2+}$ molar ratio.* A set of precipitation tests were carried out to estimate the maximum calcium precipitation without raising the pH above 10.5 to avoid/limit magnesium co-precipitation. A total volume of 5 mL of aqueous solution, containing only Ca^{2+} at the same concentration of SB solution ($[\text{CaCl}_2] = 21.5 \text{ mM}$ (2.38 g/L)), was used by adding a variable volume of the precipitant solution ($[\text{Na}_2\text{CO}_3] = 2.36 \text{ M}$ (250 g/L)). The Ca^{2+} concentration in the supernatant and the pH were monitored as function of the added volume of the precipitant from 0 to 60 μL with a step of 10 μL . It should be observed that coexisting major ions in the SB may have impact on the CaCO_3 precipitation process, but here some ions are also present (Na^+ , Cl^- , Ca^{2+} , CO_3^{2-}) that influence the precipitation through the ionic strength, and this effect was found to be negligible [24].

(ii) *Evaluation of feeding mode of the precipitant.* These tests were performed using 250 mL of SB solution. The precipitating agent was dissolved in aqueous phase and added slowly at controlled speed by means of a syringe pump (NE-1000 family of programmable syringe pumps, New Era Pump Systems Inc., Farmingdale, NY, USA) at three different flowrates (53.75, 393.5, and 465.1 $\mu\text{L}/\text{min}$) or at once in solid form (0.57 g of Na_2CO_3). The added amount of precipitant corresponded to a $\text{CO}_3^{2-}/\text{Ca}^{2+}$ molar ratio of 1.1.

(iii) *Evaluation of temperature's effect on precipitation performance.* A volume of 500 mL of SB solution was used to assess the precipitation performance at a temperature of 35 °C and 15 °C as this was the range of interest in this work. The volume of precipitant solution was first added to 100 mL portion of the SB solution and vigorously mixed via vortex for 1 minute, and then this portion was added to the remaining 400 mL of the SB solution under vigorous agitation for 5 min. Then, it was decreased to obtain a gentle agitation and the precipitation continued as well as precipitate aging. Samples of the supernatant were withdrawn at regular time interval. The stirring was stopped 10 min before each sample to avoid withdrawing the precipitate in addition to the supernatant.

To evaluate the precipitation's behavior in completely different conditions from the previous ones, some tests using a 250 mL volume of SB solution at a temperature of 60 °C were carried out. The precipitating agent ($[\text{Na}_2\text{CO}_3] = 1 \text{ M}$) was added by using the syringe pump to obtain $\text{CO}_3^{2-}/\text{Ca}^{2+}$ molar ratios of 1.1 and 1.3 with the same injection time (15 min). Thus, 5.90 and 6.98 mL of the precipitating solution were fed at rates of 393.5 and 465.1 $\mu\text{L}/\text{min}$, respectively. During the 15 min time interval, the SB solutions were maintained under vigorous agitation and precipitation started. Then the suspension was maintained under moderate agitation and precipitation in addition to precipitate

aging. Since in these tests, the precipitation rate seemed to be slowing down after 3 h, the possibility of its increase was assessed by a second injection of the precipitating solution for 15 min after 3 h.

(iv) *Evaluation of the antiscalant effect on precipitation performance.* These tests were carried out on 5 and 500 mL of SB solutions with and without presence of the Permatreat antiscalant at concentration of 2 mg/L, and different addition modes of the precipitant were also tested. In particular, the precipitant was added both in solid and solution forms, achieving a $\text{CO}_3^{2-}/\text{Ca}^{2+}$ molar ratio of 1.1. The possibility to enhance the precipitation performance was also evaluated by initial addition of CaCO_3 seeds (0.02 g of solid) into the 5 mL volume of SB solution.

(va) *Precipitation tests using a 4xCaMg solution.* To collect information on the precipitation behavior without presence of major ions, a 4x solution (4xCaMg), compared to the SB solution, was prepared by dissolving only CaCl_2 and MgCl_2 (Ca^{2+} was 86 mM and Mg^{2+} was 460 mM) in pure water. After stirring overnight, the solution was turbid, with pH of 9.03, which disappeared by addition of HCl decreasing the pH to 7.8. In some tests, a solid Na_2CO_3 form (5.015 g) was added to 100 mL of the 4xCaMg solution, and this was vigorously mixed via vortex for 5 min until the solid was dissolved. Then, 400 mL of the 4xCaMg solution was added once more under vigorous stirring to obtain a total volume of 500 mL at a molar $\text{CO}_3^{2-}/\text{Ca}^{2+}$ ratio of 1.1. Afterwards, the stirring was decreased, and the precipitation continued. In other tests, the precipitant (25 mL, $[\text{Na}_2\text{CO}_3] = 1.9 \text{ M}$) was added in solution form to 500 mL of the 4xCaMg solution at 2.5 mL/min with the syringe pump for 10 min under vigorous stirring, thus achieving a $\text{CO}_3^{2-}/\text{Ca}^{2+}$ molar ratio of 1.1. The vigorous stirring continued for 5 min and then the speed was decreased to continue the precipitation reaction.

(vb) *Precipitation tests using the 2xSB solution.* These precipitation tests were performed at 15 and 35 °C with the 2xSB solution, with the composition reported in Table 1, containing 8 mg/L of the antiscalant. A volume of 25 mL of precipitant solution ($[\text{Na}_2\text{CO}_3] = 0.95 \text{ M}$) was added to 500 mL of the 2xSB solution at 2.5 mL/min for 10 min under vigorous stirring, thus achieving a $\text{CO}_3^{2-}/\text{Ca}^{2+}$ molar ratio of 1.1. Then the stirring rate was decreased to continue the precipitation reaction.

2.4. Laboratory-Scale Plant for Calcium Precipitation

A laboratory experimental setup, reported in Figure 1, was designed and assembled on the basis of the results obtained in the preliminary tests. It consists of a brine reservoir ($V = 60 \text{ L}$), containing 50 L solution, and a Na_2CO_3 reservoir containing 1.5 L of solution (1.9 M). These solutions were fed, by means of two peristaltic pumps, to mixing tank 1 ($V = 1 \text{ L}$), where an intense mixing of the two solutions took place and the precipitation process started. Peristaltic pump 1 feeds the 2xSB solution at a flowrate of 83.3 mL/min (or 5 L/h), while peristaltic pump 2 feeds the precipitant solution at a flow rate of 2.1 mL/min (or 125 mL/h) in agreement with a molar ratio of $\text{CO}_3^{2-}/\text{Ca}^{2+} = 1.1$.

The solution contained in mixing tank 1 was vigorously stirred by a magnetic stirrer (magnetic hotplate stirrers, C-MAG HS 7, speed range of 100–1500 rpm, from IKA) and its temperature was controlled by means of a thermostat coil fed with water at appropriate temperature controlled by thermostat 1.

When mixing tank 1 is full, the supernatant falls by gravity into mixing tank 2 ($V = 15 \text{ L}$), where the precipitation process reaches its completion and the precipitate ages. The solution contained in mixing tank 2 is slightly stirred by a mechanical stirrer (VOS 40 digital electronic overhead stirrer, speed range of 30–2000 rpm, from VWR International), and its temperature is controlled by means of a thermostat coil fed with water at appropriate temperature controlled by thermostat 2. So, mixing tanks 1 and 2 can be operated at different stirring intensities and at different temperatures, if needed.

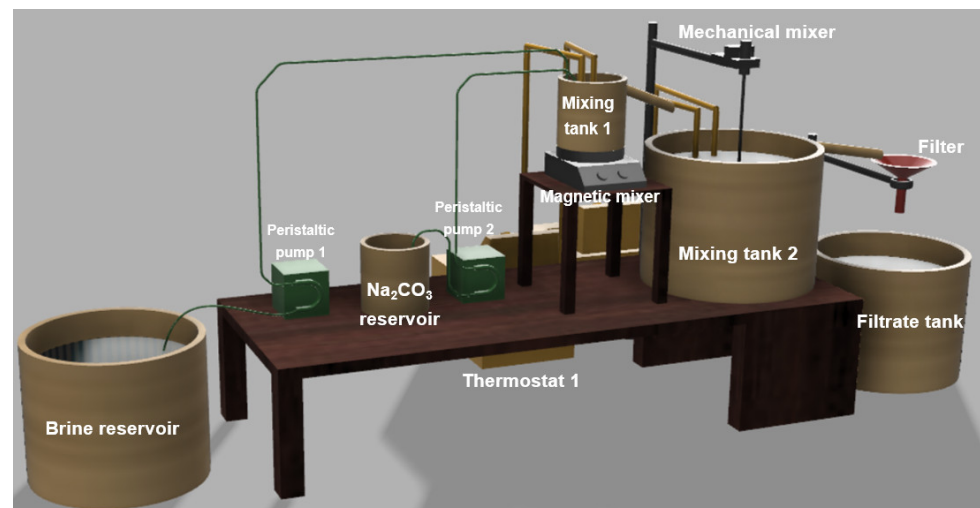


Figure 1. Schematization of the lab-scale plant used for performing the calcium precipitation tests.

The supernatant of mixing tank 2 falls by gravity into a funnel, where a filter paper separates the solid precipitate from the aqueous phase. Liquid samples are withdrawn at this time directly from the output of the filter before being mixed with the other filtrate contained in the filtrate tank.

2.5. Methodology of the Calcium Precipitation Tests for the Lab-Scale Plant

2.5.1. Precipitation Tests in Continuous Mode

A volume of 50 L of 2xSB solution of the synthetic brine, also containing minor ions at concentration in the order of 10^{-3} g/L (Table 1), was prepared as follows. The various components were dissolved under mechanical agitation (200 rpm). The pH of this solution was adjusted to 7.1 by addition of some drops of appropriately diluted HCl. Despite the addition of 8 mg/L of the antiscalant to avoid the precipitation of CaSO_4 , only very little precipitation was observed. The mass of this precipitate was negligible as it was about 73 g, which represented 1% of the total mass of the salts used to prepare the 2xSB solution (7158.75 g considering only the major ions). This precipitate was separated by filtration, and then the solution remained clear before it was used. Then, 1.5 L of 1.9 M Na_2CO_3 was prepared to be used as precipitating agent.

The start-up phase of the plant in continuous mode was as follows. Mixing tank 1 and mixing tank 2 (see Figure 1) were pre-filled with 1 L and 15 L, respectively, of 2xSB solution, and then the appropriate volume of Na_2CO_3 was added to each one to achieve a molar ratio of $\text{CO}_3^{2-}/\text{Ca}^{2+} = 1.1$ according to the results obtained in the preliminary tests. The temperature was maintained at 35 °C in both the mixing tanks by the two thermostats. Both the solutions in tanks 1 and 2 were stirred at high speed (ca. 500 rpm) for 10 min after the addition of the precipitant. Then, high-speed stirring was maintained during all the runs into mixing tank 1, to achieve an intense pre-mixing of both solutions, while the stirring speed in mixing tank 2 was decreased as necessary (ca. 150 rpm) to assure the homogeneous dispersion of the growing precipitate particles. At this point, the continuous feeding of 2xSB and $\text{Na}_2\text{CO}_3(\text{aq})$ solutions at 5 L/h and 0.125 L/h, respectively, into tank 1 started, and the operation continued for 6.5 h.

Filtered liquid samples were collected from the bottom of the filter funnel at 0, 30, 60, 120, 180, 240, 300, 360, and 390 min. The filter paper was changed at 60, 120, 180, 240, 300, 360, and 390 min, and the collected fractions of precipitate were dried in oven at 105 °C overnight.

The liquid samples were appropriately diluted with Milli-Q water and subjected to HR-CS AAS ContrAA 700 analyses. The solid samples were also analyzed after dissolution as described in Section 2.2.

2.5.2. Precipitation Tests in Batch Mode and Continuous Mode

Here, for simplicity, the minor ions were excluded as we are more interested in the behavior of the calcium and magnesium concentrations at this time. A volume of 50 L of 2xSB solution, also containing 8 mg/L of the antiscalant, was prepared as described in the previous section, except for the presence of minor ions. In this case, no precipitation was observed. The pH after correction with HCl was 6.9. In these tests, in the first 3 h, the plant operated in batch mode: 975 mL of 2xSB and 25 mL 1.9 M Na_2CO_3 were mixed into mixing tank 1, while 15 L of 2xSB and 375 mL 1.9 M Na_2CO_3 were mixed into mixing tank 2. Both solutions were stirred at high speed (ca. 500 rpm) for 10 min, then they were maintained under moderate agitation (ca. 150 rpm) for precipitate aging. The temperature was maintained at 35 °C. Starting from 3 h, the reactor was operated as a CSTR, like that in the previous section, by feeding the 2xSB and Na_2CO_3 solutions at rates of 5 L/h and 0.125 L/h, respectively, into mixing tank 1. Filtered liquid samples were collected at 0, 30, 60, 120, 180, 210, 240, 300, 360, 420, and 480 min. Precipitate samples were collected by changing the filter at 210, 240, 300, 360, 420, and 480 mins. All samples were analyzed via HR-CS AAS ContraAA 700 as described in the previous section.

2.6. Ex Ante Life Cycle Assessment

2.6.1. Goal, Scope, and System Boundaries

The LCA is a widely used methodology to quantify the potential environmental impacts of a technology [26,27]. In the present study, the goal of the assessment was to unveil and understand the critical aspects, from an environmental point of view, of the developed technology of near-ambient temperature calcium precipitation. The functional unit (FU) of an LCA is the reference flow to which the process model refers and must be representative of a quantifiable function of the process. In this study, the FU selected is the treatment (decalcification) of 100 L of RO brine (synthetic brine SB in the experiment) at an initial temperature of 25 °C. The assessment follows a cradle-to-gate approach, from resource extraction for laboratory devices, consumables, and energy production (cradle) to the precipitation process itself (gate), including process waste disposal (Figure 2). Major details of the scheme reported in Figure 2 are clarified at the end of the discussion section.

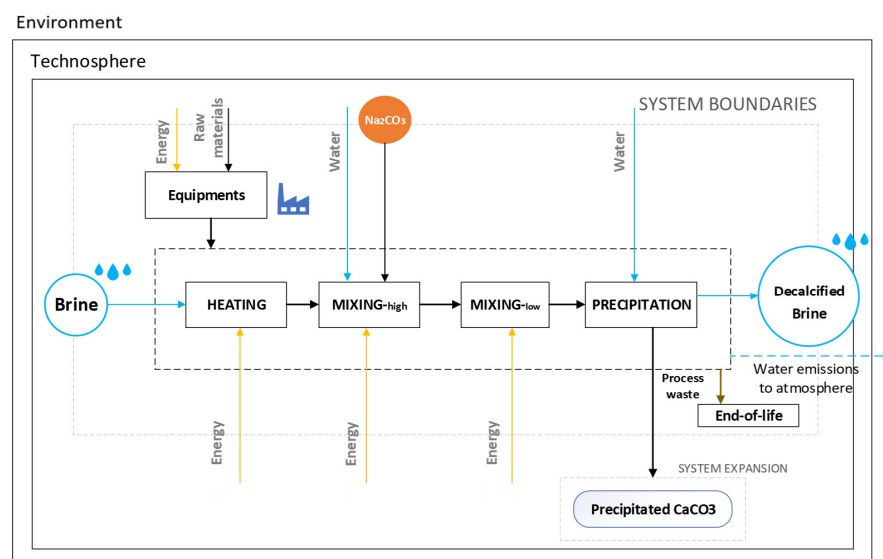


Figure 2. System boundaries of the near-ambient temperature calcium precipitation life cycle assessment (LCA).

The disposal of capital goods at the end of their lifetime is not included in this study. The LCA was conducted by using the SimaPro 9.4.0.2 software and the Ecoinvent database version 3.8, and according to the principles described in the ISO standards

(ISO 14040:2006, <https://www.iso.org/standard/37456.html>, accessed on 9 January 2024, and ISO 14044:2006, <https://www.iso.org/standard/38498.html>, accessed on 9 January 2024). Given that the process results are decalcified brine (desired product) and precipitated CaCO_3 (by-product), the “avoided product” approach is used. This approach for system expansion, as an alternative to allocation, considers the resulting by-products as alternatives to other products on the global market. In this regard, impacts related to precipitated CaCO_3 are assumed to be outside the assessed process system, and the system is credited with the impacts avoided from alternative CaCO_3 production processes.

2.6.2. Environmental Indicators

To reflect the environmental impacts of the brine treatment proposed, the midpoint indicators in Environmental Footprint 3.0 method (EF 3.0, adapted for SimaPro) were selected. This method, as adopted from Environmental Footprint transition phase of the European Commission, includes the following: climate change, ozone depletion, ionizing radiation, photochemical ozone formation, particulate matter, human toxicity (non-cancer), human toxicity (cancer), acidification, eutrophication freshwater, eutrophication marine, eutrophication terrestrial, ecotoxicity freshwater, land use, water use, resource use (fossils), and resource use (minerals and metals). Further information about the midpoint indicators and acronyms is reported in Table S1, Supplementary Information.

2.6.3. Inventory

Figure 2 and Table 2 summarize the near-ambient temperature calcium precipitation process, performed in a batch system (not working continuously), as well as the foreground data for each of the components involved in the process (i.e., energy, chemicals, laboratory equipment, waste, etc.). Major details of the components reported in Table 2 are clarified at the end of the discussion section. Assumptions and limitations of the inventory are reported in Table S2, Supplementary Information. All background data are taken from Ecoinvent version 3.8.

Table 2. Life cycle inventory (LCI) for the near-ambient temperature calcium precipitation system scenario (p: piece; values corresponding to the selected functional unit; FU: decalcification of 100 L of RO brine).

Type	Sub-Type	Component	Value	Unit
Input	Cap. Good	Thermostat	9.259×10^{-6}	p/FU
		Stirrer	5.864×10^{-5}	p/FU
		Peristaltic pump	1.688×10^{-7}	p/FU
		Tanks	5.041×10^{-5}	p/FU
	Operations	Thermostat	1.200	kWh/FU
		Stirrer _{LOW}	3.000×10^{-1}	kWh/FU
		Stirrer _{HIGH}	8.333×10^{-2}	kWh/FU
		Peristaltic pump	4.971×10^{-2}	kWh/FU
	Consumables	RO brine	1.000×10^2	L/FU
		Na_2CO_3 salt	2.500×10^2	g/FU
Water for Na_2CO_3 solution		2.500	L/FU	
Cleaning Water		1.000×10^{-1}	L/FU	
Bag filter		2.000×10^{-5}	Kg/FU	

Table 2. Cont.

Type	Sub-Type	Component	Value	Unit
Output	Wastes	Cleaning Water	1.000×10^{-1}	L/FU
		Bag filter	2.000×10^{-5}	Kg/FU
	By-product	Precipitated CaCO ₃	1.900×10^2	g/FU
	Product	Decalcified brine	1.025×10^2	L/FU

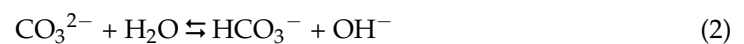
3. Theoretical Considerations for CaCO₃ Precipitation

3.1. Sodium Carbonate Concentration to Minimize Magnesium Co-Precipitation

In our previous work [24], a 2.36 M sodium carbonate concentration was used to precipitate the calcium as calcium carbonate, but about 25% Mg(OH)₂ co-precipitation was observed, which was ascribed to the high initial pH of the sodium carbonate solution (pH = 12). Using the PhreeqC equilibrium numerical code, it was shown that at pH values below 10.5, the precipitation of Mg(OH)₂ is avoided. This condition was obtained in that work by using sodium hydrogen carbonate adjusting the pH between 9 and 9.5 with NaOH. It should be observed that sodium hydrogen carbonate alone, as the hydrogen carbonate is an amphoteric ion, results in a pH = 8.3, independently from the concentration, according to the following formula:

$$[\text{H}^+] = (\text{K}_{a1} \text{K}_{a2})^{1/2} \quad (1)$$

where $\text{K}_{a1} = 4.2 \times 10^{-7}$ and $\text{K}_{a2} = 5.6 \times 10^{-11}$ are the first and second dissociation constants of H₂CO₃. If Na₂CO₃ is used as precipitant, as is the case in the present work, the CO₃²⁻ ion results in the following hydrolysis equilibrium:



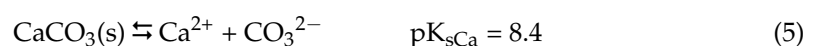
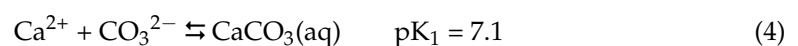
and

$$[\text{OH}^-] = (\text{K}_b \cdot \text{C}_s)^{1/2} \quad (3)$$

where $\text{K}_b = \text{K}_w/\text{K}_{a2} = 1.79 \times 10^{-4}$ is the hydrolysis equilibrium constant of Equation (2), C_s is the initial concentration of the carbonate ion in the solution, and K_w is the equilibrium constant of the ionic product of water. Equation (3) shows that, unlike the case of the HCO₃⁻ ion, the [OH⁻] and the pH depend on the sodium carbonate concentration in the solution. So, the carbonate concentration should be lowered to reduce the magnesium co-precipitation and higher to increase the CaCO₃ precipitation. Considering that in the simulated brine, the initial Ca²⁺ concentration is 21.5 mM, and considering a molar ratio of CO₃²⁻/Ca²⁺ = 1.1 (see Section 4.1), the initial [CO₃²⁻] = $\text{C}_s = 23.65$ mM, so an initial pH = 11.31 will be obtained from Equation (3) by hypothesizing instantaneous mixing just after the addition of sodium carbonate. The final pH, instead, can be estimated by hypothesizing, for example, 90% Ca precipitation, which means a final [CO₃²⁻]_f = $\text{C}_{sf} = 4.73$ mM. Then, from Equation (3) and changing from [OH⁻] to [H⁺], a pH = 10.96 can be obtained. Both the calculated (initial and final) pH values are higher than 10.5, but it must be observed that this calculation is performed considering the addition of these species to pure water. In real situations, some buffering effects and lower pH values are expected; thus, magnesium should not precipitate significantly. This aspect will be verified in the experimental tests.

3.2. Thermodynamic and Kinetic Aspects of CaCO₃ Precipitation

Sodium carbonate in water dissociates the CO₃²⁻ ion which reacts with the Ca²⁺ ion and forms a CaCO₃ aqueous complex and solid precipitate according to reactions (4) and (5):



The crystalline CaCO_3 minerals are constituted by three polymorphs, i.e., vaterite, aragonite, and calcite. Their stability is as follows, in decreasing order: calcite, aragonite, and vaterite [28], which is also confirmed by the values of the respective solubility products ($\text{p}K_s$: 8.48, 8.34, and 7.91) (<https://www.aqion.de/site/16>, accessed on 9 January 2024), meaning a lower solubility for the more stable crystals. From theoretical point of view, the crystallization process can be divided into three stages [29]: (i) induction period, during which the solute concentration remains constant and molecules of the solute agglomerate to form crystal nuclei distributed in various sizes [30]; the nuclei of largest size in this distribution are said to be critical, meaning that any further addition of solute molecules causes them to grow into crystals; (ii) growing stage, in which the solute concentration begins to decrease while, at the same time, new nuclei continue to form, and the nuclei that have already developed facets, edges, and corners increase in size to become crystals [31]; and (iii) steady-state stage, in which the solute concentration has diminished, asymptotically approaching the equilibrium solubility of the solute. Any crystals spawned at this time are too small to ever come into equilibrium with the ambient supersaturation. In a process called Ostwald ripening, these small crystals dissolve, and the solute that is released precipitates onto the larger crystals [32–36]. According to the Von Weimarn theory, the particle size of a precipitate is influenced by precipitate solubility, temperature, reactant concentrations, and the rate at which reactants are mixed. The net effect of these variables can be accounted for, at least qualitatively, by the Von Weimarn equation, assuming that the particle size is related to a single property of the system called relative supersaturation (RSS):

$$\text{RSS} = (Q - S)/S \quad (6)$$

where Q is the precipitant solute concentration at any instant, and S is its concentration at equilibrium. S can be increased by varying the temperature, by adjusting pH (if the solubility of the precipitate depends on pH), or by adding a complexing agent. Q can be decreased by using a dilute precipitating solution, adding the precipitating agent slowly and stirring, or by using homogeneous precipitation technique (the precipitating agent is synthesized in the solution rather than being added mechanically). Experimental evidence indicates that the particle size of a precipitate varies inversely with the average RSS during the time when the reagent is being introduced. Thus, when RSS is large, the precipitate tends to be colloidal (tiny particles invisible to the naked eye of 10^{-3} to $1 \mu\text{m}$ in diameter), and when RSS is small, a crystalline solid (particles greater than $1 \mu\text{m}$) is more likely to form. If Q is expressed as the solubility quotient (for CaCO_3 , this is equal to $Q_s = [\text{Ca}^{2+}][\text{CO}_3^{2-}]$) and S as the solubility product (for CaCO_3 it is $K_{s\text{Ca}}$), Equation (6) can be written as follows:

$$\text{RSS} = (Q_s - K_{s\text{Ca}})/K_{s\text{Ca}} = (Q_s/K_{s\text{Ca}}) - 1 = \text{OSR} - 1 \quad (7)$$

where $\text{OSR} = Q_s/K_{s\text{Ca}}$ is the oversaturation ratio [24]. Equation (7) shows that RSS is significantly different from OSR only in the case in which OSR is, on average, below 10–12. Indeed, in a work by Pan et al. [35], an OSR (they call this the saturation state, Ω) around 5 was used to study the effect of the presence of Mg(II) in inhibiting the nucleation process of CaCO_3 precipitation (first stage of the crystallization process). In the same work, the rate (R) of precipitation/dissolution of CaCO_3 in SW was expressed as dependence of SW OSR through the following empirical equation:

$$R = k \cdot (\Omega - 1)^n \quad (8)$$

where k is the precipitation rate constant, n is the “order” of the reaction, and $\Omega = \text{OSR}$ is the CaCO_3 oversaturation ratio. The linear logarithm form of this equation is as follows:

$$\log(R) = \log(k) + n \cdot \log(\Omega - 1) \quad (9)$$

where $\log(k)$ is the intercept, and n is the slope.

It must be pointed out that crystallization and precipitation are two separation techniques which sometimes are used interchangeably because in both methods, the end product is a solid precipitate. However, their difference is significant since the crystallization process takes more time (days) than the precipitation process, which can be near instantaneous, while their end products are different: crystals are produced in crystallization, and amorphous solids are produced in precipitation. The reason of this difference is the RSS value, which is very low in the crystallization process while it can be very high ($\gg 1$) in the precipitation process, so, in this last case, RSS and OSR values in Equation (7) are practically the same. By increasing the RSS, the rate of nucleation and the number of nuclei increase with the formation of particle size of the precipitate, which is influenced by its solubility, temperature, reactant concentrations, and rate at which reactants are mixed. Since the precipitation process is quite fast, the small solid particles can also contain some co-precipitated species. In CaCO_3 precipitation from SW desalination brines, the presence of Mg(II) in the solution (in this work, the $\text{Mg}^{2+}/\text{Ca}^{2+}$ molar ratio is 5:1) should inhibit the CaCO_3 precipitation [24,36], but, given the very high value of OSR (in this work, for a precipitation molar ratio of $\text{CO}_3^{2-}/\text{Ca}^{2+} = 1.1$, it is 127,760), the negative effect of Mg^{2+} competition on Ca^{2+} precipitation is not significant. Indeed, aragonite crystallographic form of CaCO_3 , in which Mg(II) is not incorporated, is expected [37] and can be experimentally found (see Section 4.6). Considering the three stages of the crystallization/precipitation process, as mentioned before, it can be assumed that, because of the very high initial OSR value, the precipitation of CaCO_3 carried out in this work is very fast in the first stage and then it is influenced by the second and third stages (growth and Ostwald ripening). In the work of Kawano and Hwang [38], the precipitation rate was described by the first-order kinetic model expressed in Equation (10):

$$k_1 t = \ln(\text{Co}/\text{Ct}) \quad (10)$$

where k_1 is the precipitation rate constant, t is the reaction time, and Co and Ct are the free Ca^{2+} concentrations at times zero and t , respectively. The k_1 constant can be obtained as the slope of the straight line in the plot of $\ln(\text{Co}/\text{Ct})$ vs. t .

4. Results and Discussion

Many factors, such as the ratio of $\text{Mg}^{2+}/\text{Ca}^{2+}$, temperature, dissolved organic matter (DOM), phosphate concentration, salinity, pH, etc. [39,40], may affect CaCO_3 precipitation, but, in this work, only some of them have been considered because the brine composition was fixed. Indeed, the objective was only to maximize the Ca^{2+} precipitation with minimal Mg^{2+} loss at a near-ambient temperature, by using a synthetic brine (SB) with an average composition from SWRO plants [24]. After some theoretical considerations for CaCO_3 precipitation, our results and discussion of the studied parameters are reported, including the following: the molar ratio of $\text{CO}_3^{2-}/\text{Ca}^{2+}$, the addition mode of the precipitant, temperature, the presence of an antiscalant, precipitation kinetics, the Ostwald ripening effect, the presence of minor ions, and the operation of the lab plant in continuous or batch modes. Then our evaluation of the amount of energy saved working at a near-ambient temperature versus a higher temperature and our evaluation of an ex ante LCA of the batch CaCO_3 precipitation process are reported.

4.1. Choice of the $\text{CO}_3^{2-}/\text{Ca}^{2+}$ Molar Ratio and Addition Mode of Sodium Carbonate

From Equation (4), the stoichiometric unitary molar ratio of $\text{CO}_3^{2-}/\text{Ca}^{2+}$ to precipitate the calcium as CaCO_3 can be observed. Since it is an equilibrium reaction, a molar ratio higher than one is predicted to be used to obtain maximal Ca^{2+} precipitation. However, the carbonate ion added into the solution is subjected to the hydrolysis equilibrium of Equation (2), which shows an increase in $[\text{OH}^-]$ if the concentration of the carbonate ion is increased, which means a pH increase and the risk of magnesium co-precipitation. To avoid/reduce this co-precipitation, the carbonate ion concentration should be below the

value that results in a pH of 10.5, as discussed in Section 3.1. This value has been determined in the test of Figure 3 by increasing the addition of the carbonate ion in a solution containing the calcium ion at the same concentration as that present in the simulated brine. In Figure 3, it can be observed that for a sodium carbonate addition of 46 μL (corresponding to a stoichiometric value of $\text{CO}_3^{2-}/\text{Ca}^{2+} = 1$), the pH is below 9.6, while for 50 μL (a 10% greater stoichiometric value), the pH is below 10.5, which is the critical pH value. So, a maximum ratio of $\text{CO}_3^{2-}/\text{Ca}^{2+} = 1.1$ was chosen and is employed throughout this work except for some cases (see Figure S1 discussed at the end of Section 4.2) in which a ratio of 1.3 is also used to further confirm the above-chosen value. It should be observed that the sodium carbonate amount to obtain this ratio can be added in solid form or as a solution with variable concentrations. In the first case, no volume increase in the treated brine is obtained, while in the second case, the volume increase in the treated brine depends on the concentration of the carbonate solution. The more concentrated the solution is, the less the volume increases, and vice versa. However, the more concentrated the solution is, the greater the risk of a high local concentration in the treated solution with consequent magnesium co-precipitation. For this reason, a gradual addition of the carbonate solution was tested by using a syringe pump at different flowrates as reported in Figure 4. It can be observed that the solid form results in the highest Ca^{2+} precipitation after 6 h as well as the highest Mg^{2+} co-precipitation. The gradual addition results in a sharp increase in the precipitation rate using the slowest addition rate (53.75 $\mu\text{L}/\text{min}$) and the lowest magnesium co-precipitation. However, the general results in Figure 4 indicate that the maximum Ca^{2+} precipitation percentage is obtained around 3 h for all of the studied cases, and the addition rate does not influence this value much.

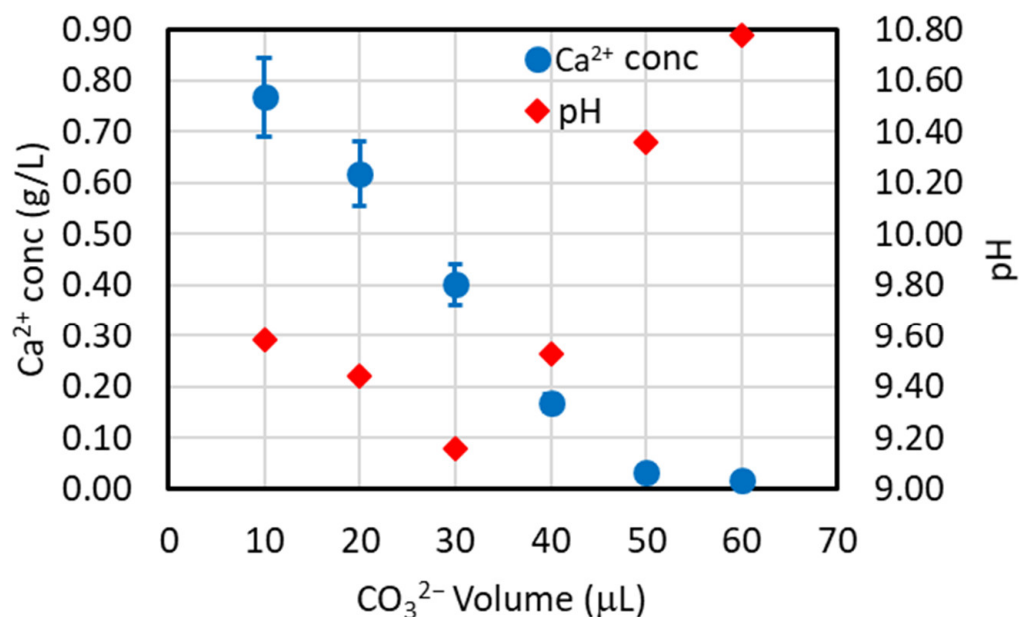


Figure 3. pH values vs. the addition of increased amount of the carbonate ion and related Ca^{2+} concentration in solution ($V_{\text{tot}} = 5 \text{ mL}$; $V_{\text{CaCl}_2} = 4.953 \text{ mL}$, $[\text{CaCl}_2] = 21.5 \text{ mM}$; $[\text{Na}_2\text{CO}_3] = 2.360 \text{ M}$, $T = 35 \text{ }^\circ\text{C}$).

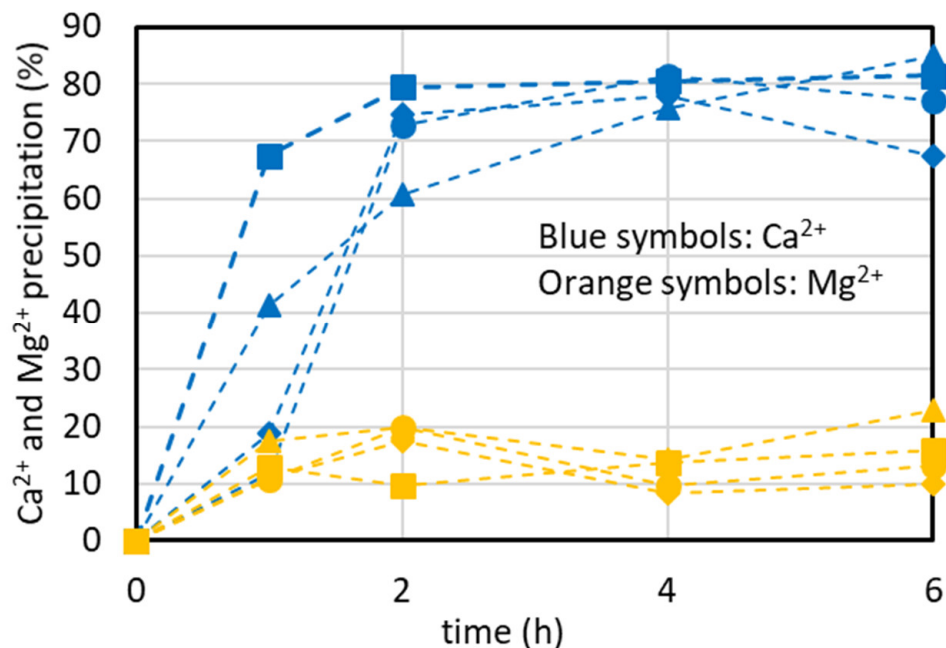


Figure 4. Precipitation percentage of Ca^{2+} and Mg^{2+} with various addition modes of sodium carbonate ($V_{\text{SB}} = 250 \text{ mL}$, $V_{\text{Na}_2\text{CO}_3, \text{added}} = 2.68 \text{ mL}$ at $[\text{Na}_2\text{CO}_3] = 2 \text{ M}$, Na_2CO_3 addition flowrate: 393.5 (●, ○), 465.1 (◆, ◇), and 53.75 (■, □) $\mu\text{L}/\text{min}$; Na_2CO_3 solid addition: 0.57 g (5.38 mmol) (▲, △), $\text{CO}_3^{2-}/\text{Ca}^{2+}$ molar ratio = 1.1; $T = 35 \text{ }^\circ\text{C}$).

4.2. Temperature's Effect on CaCO_3 Precipitation

The enthalpy variation in the dissolution of $\text{CaCO}_3(\text{s})$ in Equation (5) is negative ($\Delta H = -13.1 \text{ kJ}/\text{mol}$ at $25 \text{ }^\circ\text{C}$) [24]; thus, by increasing the temperature, the equilibrium constant decreases and the reaction shifts to the left, resulting in an increase in the CaCO_3 precipitation. However, owing to the low value of the ΔH , a low precipitation increase is expected. Indeed, the K_{ps} value at various temperatures, calculated from the value at $25 \text{ }^\circ\text{C}$ ($=3.98 \times 10^{-9}$ [24]) by using the logarithmic form of the Arrhenius equation, decreases to 2.68×10^{-9} , 1.11×10^{-9} , and 8.07×10^{-10} at 35, 60, and $70 \text{ }^\circ\text{C}$, respectively, while it increases to 6.07×10^{-9} at $15 \text{ }^\circ\text{C}$. Using these values, in Figure 5, the equilibrium curves in the temperature range of $15\text{--}70 \text{ }^\circ\text{C}$ are reported. Considering that the stoichiometric ratio of the Ca^{2+} precipitation is 1:1, a straight line with a slope of one is the precipitation path starting from the representative point of the brine after the addition of sodium carbonate with a molar ratio of $\text{CO}_3^{2-}/\text{Ca}^{2+} = 1.1$ (21.5 mM Ca^{2+} and 23.65 mM CO_3^{2-} ; not shown in Figure 5 because the scales are too large) of equation $y = x + 2.15$, where $y = [\text{CO}_3^{2-}]$ and $x = [\text{Ca}^{2+}]$. The intercept of the straight line with each equilibrium curve gives the estimation of the theoretical Ca^{2+} concentration remaining in the solution at each temperature. From this figure, it can be seen that the Ca^{2+} remaining in solution is always too small (0.004 mM at $15 \text{ }^\circ\text{C}$ and lower values at higher temperatures), so the theoretical % Ca^{2+} precipitation is practically always 100% in this temperature range. However, it should be noted that other salts are also present in the brine solution, which increase the precipitate solubility, so the expected % Ca^{2+} precipitation will be lower than 100% and practically independent from the temperature in the range of $15\text{--}70 \text{ }^\circ\text{C}$.

The above theoretical estimation is confirmed in the graph of Figure 6, where the % Ca^{2+} precipitation is always around 80–85% at 15 and $35 \text{ }^\circ\text{C}$.

The different time to reach the steady-state value in Figure 6 is ascribed to the precipitation kinetics. Indeed, the significant difference in the precipitation percentage for short periods of time (below 3–4 h) at $15 \text{ }^\circ\text{C}$ may be related to the slow precipitation kinetics at this temperature. Another justification of this lower % Ca^{2+} precipitation could be ascribed to a crystalline form of carbonate named ikaite ($\text{CaCO}_3 \cdot 6\text{H}_2\text{O}$) that usually forms at a

temperature close to the freezing point of water [40]. It is more soluble ($pK_s = 6.62$ at $25\text{ }^\circ\text{C}$, <https://www.aqion.de/site/16>, accessed on 09 January 2024) than other crystalline forms.

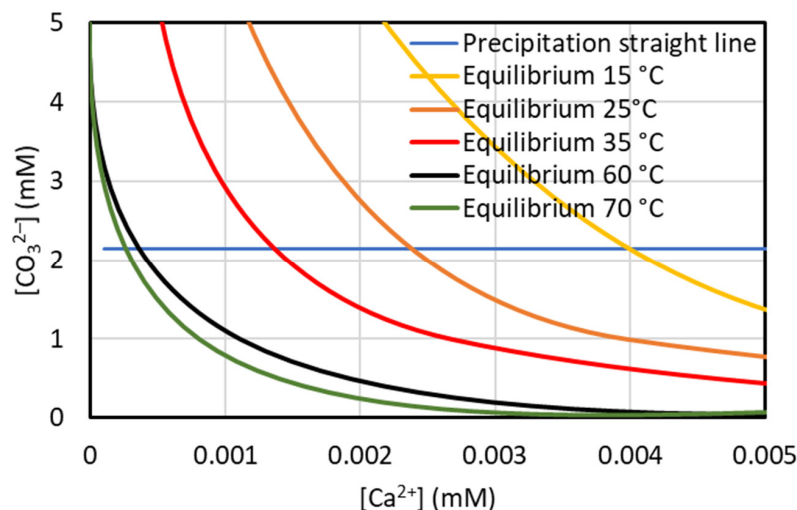


Figure 5. Theoretical estimation of the calcium concentration remaining in solution in the temperature range of $15\text{--}70\text{ }^\circ\text{C}$ for the brine used in this work and $\text{CO}_3^{2-}/\text{Ca}^{2+} = 1.1$.

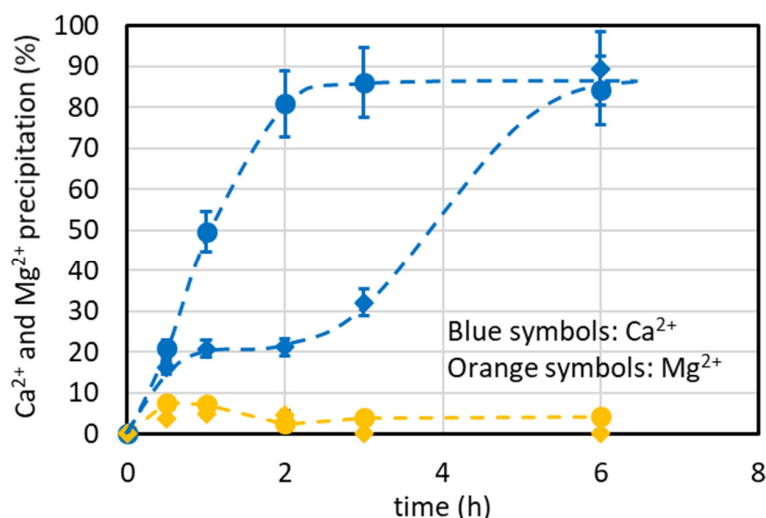


Figure 6. $\%\text{Ca}^{2+}$ and $\%\text{Mg}^{2+}$ precipitation at variable temperature vs. the time ($T = 35\text{ }^\circ\text{C}$ (●, ●) and $T = 15\text{ }^\circ\text{C}$ (◆, ◆), $V_{\text{SB}} = 500\text{ mL}$, $V_{\text{Na}_2\text{CO}_3} = 18.2\text{ mL}$ added at once, $[\text{Na}_2\text{CO}_3] = 0.65\text{ M}$, $\text{CO}_3^{2-}/\text{Ca}^{2+}$ molar ratio = 1.1).

Even though the majority of the tests were performed at $35\text{ }^\circ\text{C}$, the results of some of the tests at $60\text{ }^\circ\text{C}$, as reported in Figure S1 in the Supporting Information section, further confirmed that temperature has little effect on Ca^{2+} precipitation, as found in the theoretical estimation. In Figure S1a, a $\%\text{Ca}^{2+}$ precipitation around 80–85% can be observed, confirming, from a thermodynamic point of view, that the steady-state precipitation percentage is quite independent from the temperature. In this figure, it can also be seen that the molar ratio of $\text{CO}_3^{2-}/\text{Ca}^{2+}$ between 1.1. and 1.3 has little influence on the $\%\text{Ca}^{2+}$ precipitation, while in Figure S1b, the precipitation percentage increases to around 90% after a successive addition of carbonate, but the Mg^{2+} co-precipitation increases to unacceptable values (around 30%). The small increase in the $\%\text{Ca}^{2+}$ precipitation agrees with our theoretical calculations, as reported in Section 3.2. Indeed, the OSR is already too high (127,760) for a precipitation molar ratio of $\text{CO}_3^{2-}/\text{Ca}^{2+} = 1.1$. Because the temperature does not significantly influence the Ca^{2+} precipitation percentage, these last results also confirm the chosen molar ratio of $\text{CO}_3^{2-}/\text{Ca}^{2+} = 1.1$, as reported in Section 4.1.

4.3. Antiscalant's Effect on CaCO_3 Precipitation

Antiscalants are scale inhibitors specially used for reverse osmosis (RO), nanofiltration (NF), and ultrafiltration (UF) systems to delay the precipitation of calcium and magnesium ions on the membrane surface and prevent membrane fouling, thus improving water production and water quality and reducing operating costs [41,42]. Antiscalant/dispersant products are available as concentrates or solid powders, and dilution is required to obtain a typical dosage of 2–5 mg/L. The action mechanisms of antiscalants can be different: (i) Ca^{2+} forms a water-soluble complex or chelate with an antiscalant, so that the solubility of inorganic salts increases and consequently insoluble salts can exceed the saturation solubility in concentrated water; (ii) lattice distortion: some functional groups in the molecule of the antiscalant occupy a certain position in the inorganic salt nuclei or microcrystals, which hinders and destroys the normal growth of inorganic salt crystals and slows down the growth rate of crystals, thus reducing the formation of salt scaling; and (iii) the electrostatic repulsive effect: an antiscalant dissolved in water adsorbs the microcrystals of inorganic salts, so that the repulsive force between particles increases, hindering their agglomeration and promoting the dispersed state, thus preventing or reducing the formation of scaling. It must be observed that antiscalants act during stage 1 of the crystallization process described in Section 3.2., but, in the present work, it is expected that their presence does not inhibit the Ca^{2+} precipitation because of the very high OSR. Indeed, our experimental results for the Ca^{2+} precipitation in a 5 mL test tube, presented in Figure 7, show practically no difference with and without an antiscalant. In the same graph, the results of the addition of CaCO_3 seeds to eventually increase the precipitation kinetics are also reported, but effects can not be seen because the seeds act on stage 1 (nucleation), which is negligible in this work. The results of a 500 mL batch in the presence of the antiscalant (Figure S2, Supporting Information) and using three addition modes for the precipitant show a behavior independent from the addition mode, and the precipitation trend is very similar to that of the data presented in Figure 4 in the absence of an antiscalant. The findings reported here are not in conflict with the conclusions of some other papers (e.g., [43]), which state that antiscalants exhibit uniquely time-dependent effects on the inhibition of the formation of a calcium solid. Indeed, the precipitation kinetics exhibits a three-phase behavior, with an induction phase, a rapid reaction phase, and a final equilibrium phase. In the present work, as observed before, the induction phase is negligible because of the high OSR, so the antiscalant's presence did not influence the equilibrium phase which determined the % Ca^{2+} precipitation. Though antiscalants are removed before further brine processing [44,45], this aspect was not considered.

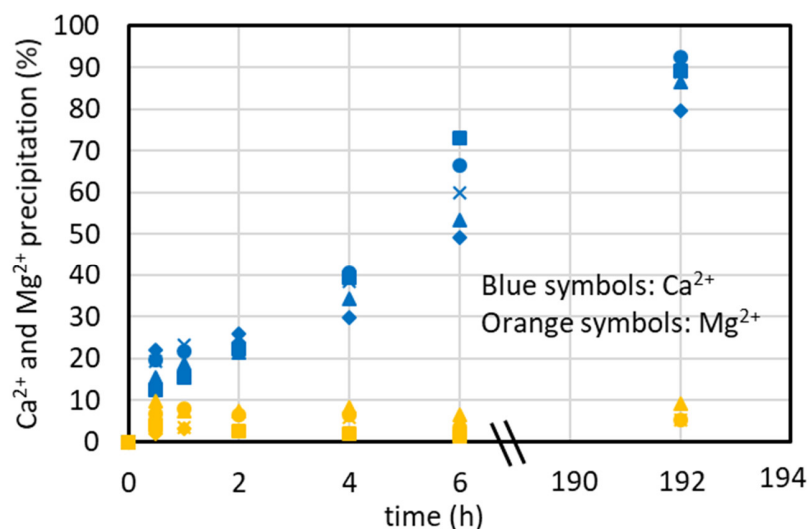


Figure 7. Antiscalant's effect on % Ca^{2+} and % Mg^{2+} precipitation vs. time. $V_{\text{SB}} = 5$ mL, without antiscalant: Na_2CO_3 added at once as 0.65 M solution (181.64 μL) (\bullet , \circ), Na_2CO_3 added as solid

(0.0125 g) (◆, ◇), 0.4% CaCO₃ seeds and Na₂CO₃ added at once as 0.65 M solution (181.64 μL) (x, x). With 2 mg/L antiscalant (Permatreat™ PC-1020): Na₂CO₃ added at once as 0.65 M solution (181.64 μL) (▲, ▲), Na₂CO₃ added as solid (0.0125 g) (■, ■); CO₃²⁻/Ca²⁺ molar ratio = 1.1, T = 35 °C.

4.4. Effect of Initial Concentration of the Synthetic Brine on CaCO₃ Precipitation Kinetics

The results described in the previous sections always show a time around 3 h to achieve the maximum %Ca²⁺ precipitation. When transferring the results from the laboratory scale to an industrial scale, a reduced equipment size (and thus capital and operating costs) is required if fast kinetics is obtained. It is expected that if the initial Ca²⁺ concentration increases, the precipitation kinetics increases too. In the following, some considerations for the choice of the maximum brine concentration to carry out the Ca²⁺ precipitation are reported. Because a real 4xSB solution resulted in CaCO₃ and CaSO₄ precipitation, some preliminary precipitation tests were performed for a 4xCaMg solution containing only CaCl₂ (86 mM) and MgCl₂ (460 mM) according to the methodology described in Section 2.3, paragraph *v_a*. The results, reported in Figure 8, show that the time to obtain the maximum %Ca²⁺ precipitation is still 2–3 h, like in the tests at a lower concentration using the simulated brine with the major ions, and that the maximum %Ca²⁺ precipitation is still 80–85%, showing that the free ions in solution (Na⁺, Cl⁻, Ca²⁺, Mg²⁺, CO₃²⁻) result in an effect similar to that of the major ions and confirming that the variation in ionic strength has little effect, as found elsewhere [24]. Because the %Ca²⁺ reduction reported in the graphs is normalized by the initial concentration, the trend of the curves in Figure 8 does not show an increase in the reaction rate.

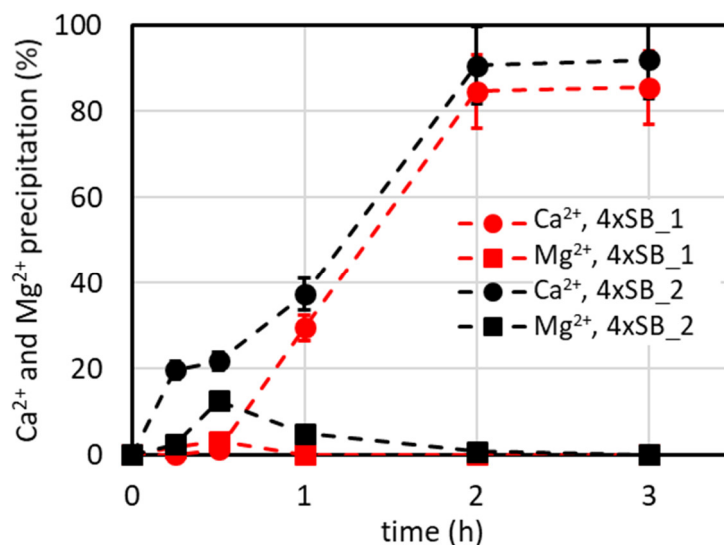


Figure 8. %Ca²⁺ and %Mg²⁺ precipitation over time using a concentrate solution containing CaCl₂ and MgCl₂ only at four different times ($V_{4x\text{CaMg}} = 500$ mL, $[\text{CaCl}_2] = 86$ mM, $[\text{MgCl}_2] = 460$ mM, Na₂CO₃ addition as solid: 5.015 g added in run 4xSB_1; Na₂CO₃ addition in solution: 25 mL, 1.9 M at 2.5 mL/min for 10 min in run 4xSB_2; CO₃²⁻/Ca²⁺ ratio = 1.1, T = 35 °C).

However, it must be observed that the precipitate amount is about four times that of the SB, so the productivity (amount of precipitate/time), and thus the reaction rate, is quadrupled according to the first-order kinetic law. Considering this potential advantage, we tested whether a 4xSB solution could be used as an initial solution by the addition of a suitable antiscalant dose. Significant precipitation was observed after mixing the components, resulting in a %Ca²⁺ remaining in solution of about 26% even when the antiscalant concentration was raised to 50 mg/L. Then the concentration was decreased to 3xSB and the %Ca²⁺ remaining in solution was about 50% with an antiscalant concentration

of 36 mg/L. A further reduction to 2xSB, using 8 mg/L antiscalant, resulted in the %Ca²⁺ remaining in solution being about 94% (also using 16 and 24 mg/L antiscalants). So, only this solution was then used for the precipitation tests in the lab plant because it could be produced by processing the SB in an NF plant as reported below. It must be observed that for the 4xSB, the $OSR_{CaCO_3} = 35,280$ and the $OSR_{CaSO_4} = 848$, meaning that all carbonate ions precipitate as CaCO₃ and some sulphate ions precipitate as CaSO₄, as the sulphate is in stoichiometric excess compared to Ca²⁺ (see Table 1 in which the values must be multiplied by two to obtain the concentration of the 4xSB). These results show that the antiscalant is effective only when the OSR is not very high (as is the case of 2xSB), and it means that at the maximum, we predict a double concentration of the SB by adding 8 mg/L antiscalant in a nanofiltration process and by recovering 50% permeate (which is a source of further potable water) and 50% retentate for which the Ca²⁺ precipitation process can be applied to produce a low Ca²⁺ stream which can be further processed for recovering metals and minerals from SW. So, to simulate this, the 2xSB solution (Table 1) was used in some precipitation tests at 35 °C and 15 °C, and the results are presented in Figure 9. The different precipitation tendencies of Ca²⁺ depending on the time at 35 °C and 15 °C in this graph are explained in Section 4.2 in the caption for Figure 6.

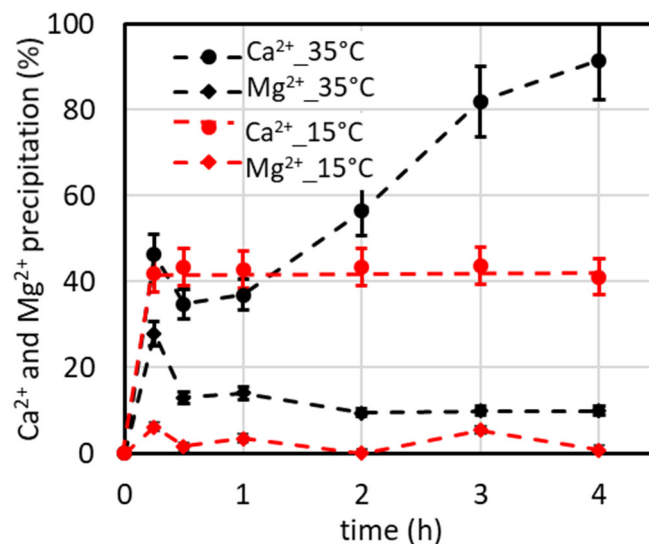


Figure 9. %Ca²⁺ and %Mg²⁺ precipitation over time using a 2xSB solution at 15 and 35 °C ($V_{2xSB} = 500$ mL, Na₂CO₃ addition: 25 mL, [Na₂CO₃] = 0.95 M, 2.5 mL/min for 10 min; CO₃²⁻/Ca²⁺ ratio = 1.1).

All our data on the %Ca²⁺ precipitation over time, as reported in the previous graphs, can be correlated by a theoretical equation considering that the second and third stages (growing and Ostwald ripening) can be described by a first-order kinetic model [38]. Instead of using the logarithmic form of Equation (10) for the first-order kinetic law ($-dC/dt = k_1 C$), the exponential form can be used as follows:

$$C = C_0 \exp(-k_1 t) \quad (11)$$

Then, by combining %Ca²⁺ precipitation/100 = (C₀ - C)/C₀ with Equation (11), we obtained the following:

$$(C_0 - C)/C_0 = 1 - C/C_0 = 1 - \exp(-k_1 t) \quad (12)$$

The first member in Equation (12) is the Ca²⁺ precipitation (%) / 100 related to Figure 9 and all the other graphs, while k_1 (h⁻¹) is the first-order kinetic constant that can be estimated from the slope of the linear trend in the plots of $\ln(C_0/C_t)$ vs. t (Equation (10)) by

elaborating on the data in these graphs. Because stage 1 (nucleation) is negligible as well as the first hour after the addition of the precipitant, which is influenced by its addition mode, the time interval of 1–6 h has been considered to estimate the average kinetic constant k_1 of the precipitation process. Furthermore, it is dependent on the temperature, so only the data at 35 °C have been considered. The average calculated k_1 value at 35 °C is $0.582 \pm 0.141 \text{ h}^{-1}$ over the time interval of 1–6 h, which can be used in the design of the Ca^{2+} precipitation process in the pretreatment of RO brine.

4.5. CaCO_3 Precipitation in Presence of Minor Ions

To simulate a real brine solution, some precipitation tests were carried out on the SB solution containing all the major and minor ions present in the SW. The concentration of each ion was practically half of the values reported in Table 1 (which refer to the 2xSB solution). The precipitation tests were performed at 15 and 35 °C (Figures S3 and S4, Supporting Information), resulting in Ca^{2+} and Mg^{2+} precipitation percentages similar to those obtained in the precipitation tests without the minor ions. In Table 3, a summary of the results at 6 h is reported. A low precipitation percentage of the Mg^{2+} and of the minor ions Li^+ , B^{3+} , Rb^+ , and Mo^{6+} can be observed. While for V^{5+} , no precipitation was observed, for Sc^{3+} , In^{3+} , and Ga^{3+} , the concentration values in the samples were lower than the detection limit of the analytical instrument. The Sr^{2+} was precipitated at about 50% according to the low solubility of SrCO_3 . These results show that only Ca^{2+} is practically precipitated while the other ions remain in the supernatant solution to be recovered more or less selectively by successive treatments with minimal difficulties due to the low concentration of the remaining calcium.

Table 3. Precipitation percentages obtained after 6 h in the CaCO_3 precipitation in presence of minor ions ($V_{\text{SB}} = 500 \text{ mL}$, Na_2CO_3 addition: 18.2 mL, 0.65 M, 1.82 mL/min for 10 min; $\text{CO}_3^{2-}/\text{Ca}^{2+}$ ratio = 1.1, $T = 15 \text{ }^\circ\text{C}$ for CO3_38 test and $T = 35 \text{ }^\circ\text{C}$ for CO3_39 test).

Test	% Ca^{2+}	% Mg^{2+}	% Na^+	% Li^+	% B^{3+}	% Sr^{2+}	% Rb^+	% V^{5+}	% Sc^{3+}	% In^{3+}	% Mo^{6+}	% Ga^{3+}
CO3_38	82.6	5.1	0.0	5.6	7.3	51.4	3.4	0	N.D. (*)	N.D.	7.1	N.D.
CO3_39	81.3	4.5	0.0	5.6	5.5	45.1	1.0	0	N.D.	N.D.	5.3	N.D.

Note: (*) N.D. Not detectable.

4.6. Ostwald Ripening's Effect on CaCO_3 Precipitation Selectivity

As mentioned in Section 3.2, precipitation reactions are faster than crystallization; thus, precipitate particles, which are obtained at the beginning of the precipitation process, can also incorporate other ions. In this case, Mg^{2+} ions particularly can enter into the CaCO_3 crystal lattice because of the five to one molar ratio of $\text{Mg}^{2+}/\text{Ca}^{2+}$ in the SB and the high local precipitant concentration just after its addition. So, the next stage of the digestion or aging of the precipitate, known as Ostwald ripening [33,34], is very important in the present work to increase the precipitation selectivity of calcium compared to that of magnesium. As recommended by IUPAC in 2007, Ostwald ripening is defined as “dissolution of small crystals or sol particles and the re-deposition of the dissolved species on the surfaces of larger crystals or sol particles”. The smaller particles, being less energetically favored than larger particles, give rise to an apparent higher level of solubility so they solubilize and then coalesce in more energetically favored, larger particles. In this process, the diffusion of ions from the disperse phase through the continuous phase occurs [46]. In particular, the solubility of the matter within a small particle (or in regions with a small curvature radius) in the surrounding continuous phase increases as the radius decreases. Because the dispersed phase has a higher level of solubility around the smaller particles, the ions solubilized from this phase move to larger particles owing to this concentration gradient, and larger particles grow at the expense of smaller ones. This mass transfer process is governed by ion diffusion according to the Stokes–Einstein equation for spherical particles

through a liquid with a low Reynolds number (as is the case of the low stirring rate applied in the aging process):

$$D = k_B T / 6 \pi \eta r \quad (13)$$

where k_B is the Boltzmann constant, T the absolute temperature, η the dynamic viscosity, and r the radius of the spherical particle. Considering that the hydrated radius of Mg^{2+} is 4.76 \AA while that of Ca^{2+} is 2.95 \AA [24], from Equation (13), it is deduced that Mg^{2+} ions released in the dissolution of the smaller particles are less likely to enter into the larger crystals because of the lower diffusion rate and remain in solution. Indeed, in the graphs of Figures 4 and 7–9, it can be observed that the $\%Mg^{2+}$ precipitation has the highest value around the first hour from the start of the precipitation and then it decreases for a longer time thanks to Ostwald ripening. The granular precipitates in the tests at 15 and 35 °C, related to the runs reported in Figure 9 taken at 4 h, were observed under a scanning electron microscope (SEM). The SEM micrography (Figure 10) shows a very different morphology with the temperature evidencing numerous and small particles with narrow and long shapes (average size of $2 \times 8 \text{ \mu m}$) at 35 °C compared to a lower number of bigger spherical particles (average diameter of 10 \mu m) at 15 °C. The X-ray diffraction and FSEM-EDAX analyses showed a prevalence of the Ca content (average weight ratio of $Ca/Mg = 9.23$) in the smaller particles at 35 °C (meaning $CaCO_3$ mainly), while a significant Mg content (average weight ratio of $Ca/Mg = 0.86$) was present in the spherically shaped particles at 15 °C. These data can be explained considering that at a low temperature (here 15 °C), the particle dissolution and ion diffusion are slow, so the Ostwald ripening effect is negligible, while at 35 °C, this effect causes $CaCO_3$ crystals to form, which are detected as aragonite.

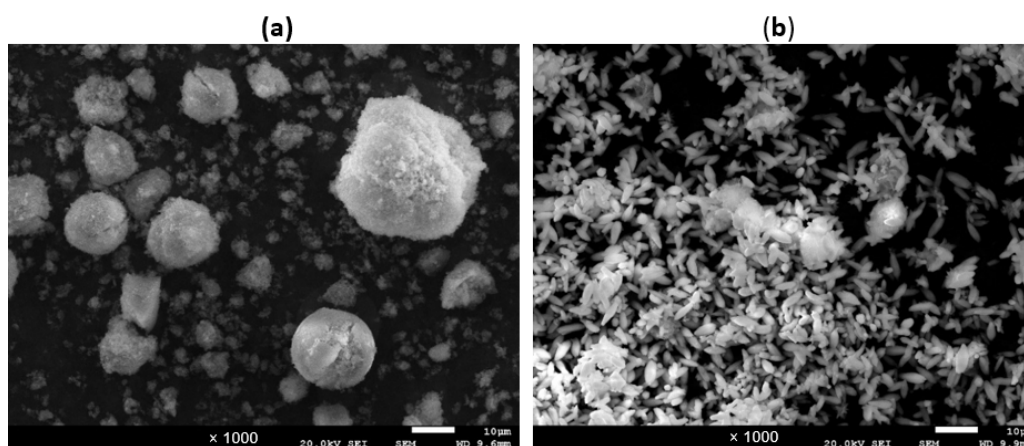


Figure 10. Scanning electron micrography of the precipitate samples collected at the end of the tests at 15 °C (a) and 35 °C (b) reported in Figure 9.

4.7. $CaCO_3$ Precipitation Tests in the Lab-Scale Plant

Based on the previous results, a laboratory plant for $CaCO_3$ precipitation, able to work in continuous or in batch modes, was designed, built, and tested (see Figure 1). In the following, the results of the plant running in the two operation modes are reported and discussed. In both cases, the 2xSB solution with the composition shown in Table 1 was used and an antiscalant was also added (8 mg/L according to the finding reported in Section 4.4). Although these tests were made with the 2xSB solution, the plant can operate with brines at a lower concentration by simply adjusting the operating parameters according to the results discussed above. The $CaCO_3$ precipitate was easily removed from the treated brine by using a laboratory filter paper. However, as the average size of the obtained $CaCO_3$ precipitate was $2 \times 8 \text{ \mu m}$ (see Section 4.6), a commercial filter bag with a pore size of 1 \mu m can be employed for practical purposes.

4.7.1. Lab-Scale Plant Operated in Continuous Mode (Including Minor Ions)

In this operating mode, the lab plant for CaCO_3 precipitation, as schematized in Figure 1, was fed at a constant rate of 5 L/h of the 2xSB solution and 0.125 L/h of the precipitant. Because the plant was empty at the beginning, the start-up procedure described in Section 2.5.1 was applied. The results reported in Figure 11 show a maximum % Ca^{2+} precipitation at 4 h (ca. 90% Ca^{2+} precipitation and ca. 5% Mg^{2+} coprecipitation), then the percentage starts to decrease as the pH remains constant at about 8.8, meaning there is a constant concentration of the precipitant (CO_3^{2-}). This means that after 4 h, an increase in the Ca^{2+} concentration in solution over time indicates a lower CaCO_3 precipitation rate. The cause of this could be the open reactor run mode and, in particular, the residence time of the Ca^{2+} ions within the reactor, which is lower than the time needed for precipitate particle growth. In continuously stirred tank reactors (CSTRs), the residence time (τ) (which is the average amount of time a molecule spends inside the reactor from the time it enters the reactor until the time it leaves) is greater than that found in the batch tests. However, we did not investigate this aspect further, and it could be of interest for the scaling-up of the continuous system.

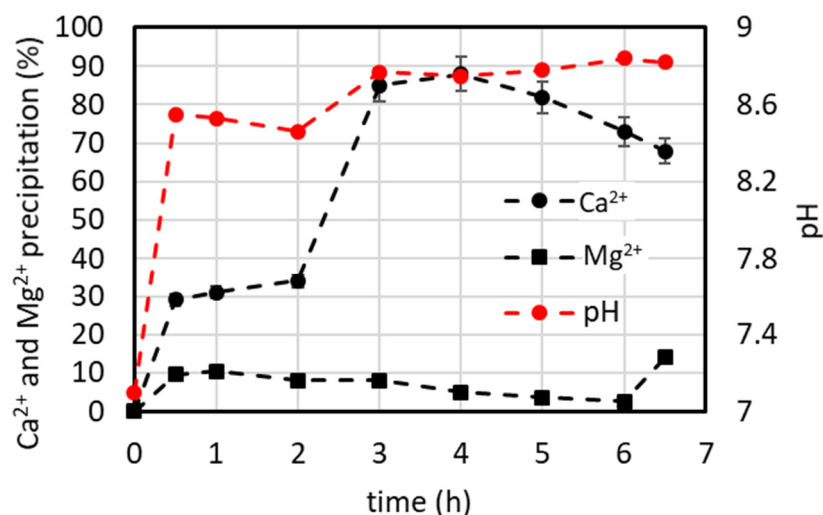


Figure 11. % Ca^{2+} and % Mg^{2+} precipitation vs. time obtained in the lab-scale plant operated in continuous mode by feeding the 2xSB solution (see details in Section 2.5.1).

Samples of the precipitate were collected over time, and the Ca and Mg content was analyzed by AAS according to the method described in Section 2.2. The weight ratio of Ca/Mg was calculated and is reported in Figure 12. The best performance is observed at 5 h (with a Ca/Mg weight ratio higher than 14), corresponding to a calcium carbonate purity of ca. 94%.

4.7.2. Lab-Scale Plant Operated in Batch and Continuous Modes (Excluding Minor Ions)

The first part of this test followed the same criteria used in the preliminary batch tests as described in Section 2.5.2. The results reported in Figure 13 show that, for the first 3–4 h, the same trend was obtained in the preliminary tests at a lower laboratory scale with lower solution volumes. After that time, a small decrease in the % Ca^{2+} precipitation starts, which can be ascribed to the switch from the batch mode to the continuous mode 3 h from the beginning. As already evidenced in the discussion of Figure 11, this can be ascribed to the higher residence time needed in the continuous system. However, here, the effect is less pronounced because the continuous mode starts at 3 h and until this time, the reactor operates in the full batch mode. The % Mg^{2+} precipitation reported in Figure 13 is quite small compared to that of Figure 11. This reflects a disturbance of the Ostwald

ripening process in which the fresh solution is fed in the continuous system compared to the batch system.

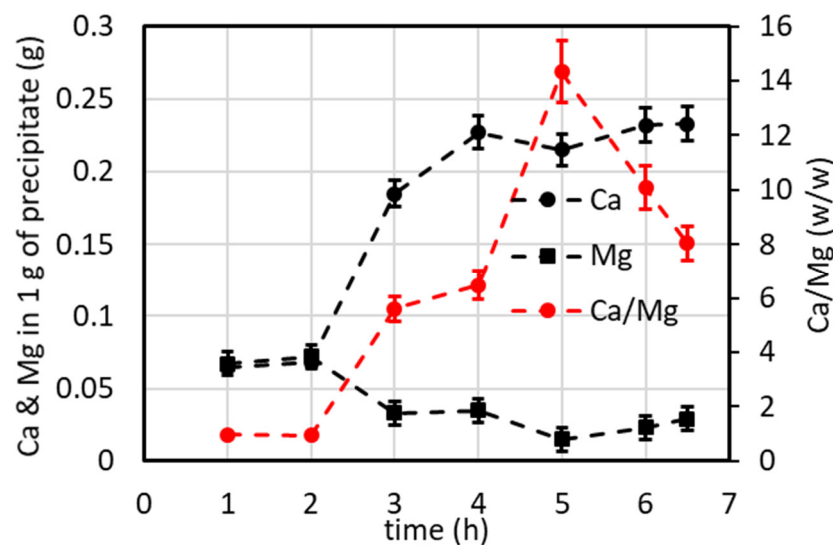


Figure 12. Mass of calcium and magnesium per gram of precipitate and Ca/Mg mass ratio vs. the collection time of the precipitate related to Figure 11.

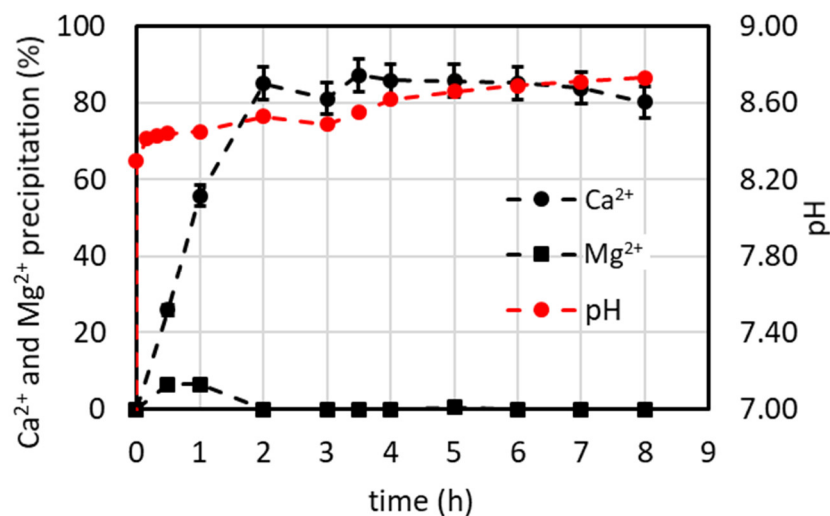


Figure 13. %Ca²⁺ and %Mg²⁺ precipitation vs. the time obtained in the lab-scale plant operated first in batch mode (till 3 h) and then in continuous mode by feeding the 2xSB solution (see details in Section 2.5.2).

In this case, samples of precipitate were also collected over time and analyzed by AAS. The weight ratio of Ca/Mg was calculated and is reported in Figure 14. The best performance was observed at 7 h (with a Ca/Mg weight ratio higher than 40), corresponding to a higher purity of calcium (ca. 97 %) compared to that of the overall continuous system.

4.7.3. Conceptual Method of the Process of Selective Ca²⁺ Precipitation

All the obtained experimental data can be summarized in a conceptual scheme of the process for selective calcium precipitation from RO brine. The main steps of this method, included in Figure 2 for the LCA analysis (see also Figure S5, Supporting Information), are as follows: (i) heating the brine to 35 °C, (ii) the addition of the precipitant under a high stirring rate, (iii) stirring all suspensions with a low stirring rate to promote the aging of the precipitate (Ostwald ripening), and (iv) the filtration of the suspension to separate the

precipitate from the supernatant (low-Ca²⁺ treated brine). With reference to this flowchart, all parts of the process and an estimation of the heating and stirring power to treat 100 L of batch RO brine are reported in Table 2 for the life cycle inventory.

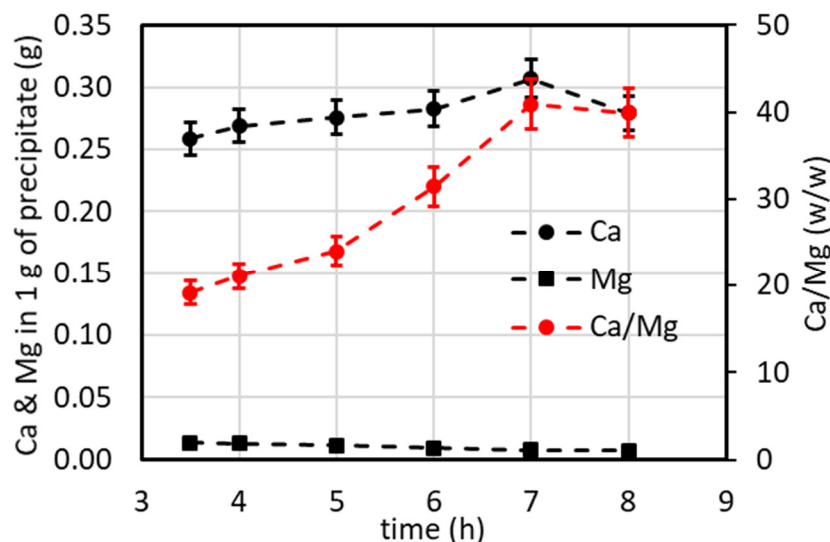


Figure 14. Mass of calcium and magnesium per gram of precipitate and Ca/Mg mass ratio vs. the collection time of the precipitate related to Figure 13.

4.8. Estimation of the Energy Saved in Ca Precipitation at Low vs. High Temperatures

In two works on CaCO₃ precipitation [24,25], temperatures of 70–85 °C were used, but this means heating the brine with consequent energy consumption. As the flowrate of RO brine to be treated in a real case is of the order of a thousand cubic meters per day, to save energy, the performance of the precipitation process at temperatures close to ambient temperature has been investigated in this work. The advantage of working at a temperature around ambient temperature is that more energy is saved when heating the brine. The obtained experimental data reported previously show that at 35 °C, the maximum %Ca²⁺ precipitation is almost the same as that at 60 °C, and in both cases, the time to reach this value is about 3 h. So, the energy saved can be estimated by comparing the energy required to heat the brine at 60 °C and 35 °C, assuming the brine has an initial temperature of 25 °C. The estimation can be made by using the following equation:

$$Q = F d c_p \Delta T \quad (14)$$

where Q is the required heat (kJ), F is the brine volumetric flow rate (m³), d is the average density (kg/m³), and c_p is the average specific heat (kJ/kg °C) in the temperature range ΔT (°C). It can be assumed that $F = 1$ m³, while the overall temperature range of interest will be 25–60 °C with the average values of d and c_p obtained from the graphs of Figures 3 and 5 from the work of Sharqawy et al. [47]. The salinity to enter in these graphs is 71.5‰ (calculated by totalling the salt concentrations in the SB, Table 1 of a previous work [24]), so $d = 1044$ kg/m³ and $c_p = 3.85$ kJ/kg °C. Then, the heat used for heating the brine from 25 °C to 35 °C and to 60 °C is 40,194 and 140,679 kJ/m³, respectively, so an energy increase of 350% can be observed. This energy saved by operating at 35 °C, rather than at 60 °C, is very significant. It is interesting to observe that, even though water is the substance with the highest specific heat (for pure water, it is 4.18 kJ/kg °C at 25 °C), its value decreases with increases in salinity, which means the more concentrated the brine is, the less heat is required.

4.9. Life Cycle Impact Assessment

The results of the life cycle impact assessment (LCIA), which converts the different flows of the inventory data into environmental impacts, are summarized in Table S3 (Supporting Information) and Figure 15. As can be seen, energy consumption (operations) is the major actor for most of the impact categories considered and ranges depending on the impact category from 32.29% to 98.27% of the total impact of the assessed process. Although near-ambient-temperature calcium precipitation shows significantly lower heating energy consumption, as estimated in Section 4.8, electricity consumption (mainly by the thermostat) remains the major impact contributor to the precipitation process. However, in the case of an industrial application, waste-heat-to-power strategies such as waste steam recovery from other processes could be considered. So, even though heating the brine from 25 °C to 35 °C seems to be the largest energy consumer and therefore is mainly responsible for the brine's environmental impact, it should result in less impact at a large scale. This is a great opportunity to considerably reduce the impact of the process in industrial environments where the use of waste heat could be coupled to the process or more efficient heating technologies could be adopted. In addition, it should be noted that technologic, climatic, and seasonal variations affect the output temperature of RO brines to be treated, therefore increasing or decreasing the energy consumption needed for the near-ambient-temperature calcium precipitation. In that sense, brine resulting from membrane-based technologies is at ambient SW temperatures, and brine produced by thermal-based technologies is 1.37–1.82 times higher [48,49]. In addition, the climatic and seasonal variations could result in a higher energy demand in high-latitude regions and during cold months in low- and middle-latitude regions, while there might be lower or no energy demand in warm months of low- and middle-latitude regions. Following energy consumption, consumable usage represents the second largest contributor to the environmental impact, resulting from near-ambient-temperature calcium precipitation, with the consumption of Na_2CO_3 being the most responsible for the environmental impact. However, if the Ca precipitation plant is located near a CO_2 -emitting process, the reaction between CO_2 and NaOH for the in loco production of this consumable could be considered. The remainder of the flows considered within the system boundaries result in a negligible impact compared to that of those already discussed. In the case of the precipitated CaCO_3 , which is assessed considering the avoided product approach, depending on the impact category, the environmental impacts credited range from 1.46% to 21.40% of the total impact of the process. Thus, the potential market adoption of the precipitated CaCO_3 which would result in the displacement of mineral CaCO_3 , thus avoiding the environmental impact deriving from its mining, results in a decrease in the impact of the assessed process (see column "Total, with AP-approach" in Table S3, Supporting Information).

It must be clarified that the presented LCA study is only the first of successive assessments that will study the environmental impact of a multi-mineral modular brine mining process. In such a modular process, brine decalcification is a crucial step which enables the functioning of the rest of process, a reduction in scaling problems, an increase in the service life of equipment and calcium's competition with ions of interest, and the valorization of RO brine. This valorization will minimize the brine's discharge into the sea and consequently will reduce the direct environmental impact of brine, which can be harmful to the sea discharging area due to its salinity, temperature, and chemical substance content [5].

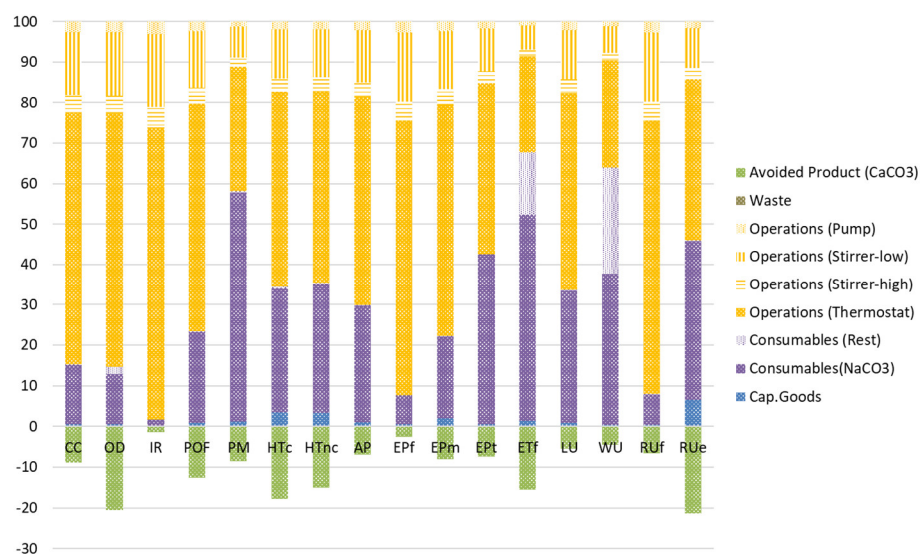


Figure 15. Relative environmental impact shares of the near-ambient-temperature calcium precipitation process (See Table S1, Supporting Information for impact category acronyms).

5. Conclusions

The valorization of very concentrated salty solutions like RO brines requires a prior treatment in order to use them as sources of metal and minerals as well as to recover further desalted water. The brine pre-treatment studied herein, by means of selective calcium removal at a near-ambient temperature, allows us to recover calcium as CaCO_3 . The precipitation process was possible at 35°C , and the control of pH levels together with the Ostwald ripening process were very important for obtaining a selective calcium precipitation. The first-order average kinetic constant of the precipitation at this temperature was $0.582 \pm 0.141 \text{ h}^{-1}$. The presence of minor ions as well as an antiscalant did not influence the precipitation; the average $\%\text{Ca}^{2+}$ precipitation was 90% while the Mg^{2+} co-precipitation was lower than 5–7%. Our tests in a lab-scale plant, operated in continuous (5 L/h synthetic brine) and in batch (15 L) modes, showed that the latter performs better. Our estimation of energy requirements showed a significant amount of energy saved (350%) when operating at 35°C compared to 60°C . The Ostwald ripening process with an “aging” time of 3 h allowed us to achieve the goal of the proposed process by selectively removing about 90% of the calcium. The treated concentrate solution with a low calcium content can be further treated to recover water and minerals without scaling difficulties related to calcium precipitation, which is the major obstacle encountered when treating SWRO brine to recover water and minerals. These results are very interesting since the removal of calcium is preparatory for designing an NZLD process for brine valorization treatments. The ex ante LCA referring to the batch mode (100 L) showed that the main environmentally impactful factors in the lab-scale plant configuration were the thermostatic heating and the addition of a precipitant (Na_2CO_3). However, in an industrial configuration, other heating sources as well as the in loco production of Na_2CO_3 from CO_2 emissions and NaOH could improve the environmental performance of the process. The near-ambient-temperature calcium precipitation process has a low environmental impact compared to that of others that need to reach higher temperatures through energy consumption.

Supplementary Materials: The following supporting information can be downloaded at: <https://www.mdpi.com/article/10.3390/w16050667/s1>. Table S1. Impact category indicators use in the life cycle assessment and their acronyms. Table S2. Life Cycle Inventory (LCI) assumptions and limitations for the near-ambient temperature calcium precipitation system scenario. wh: working hours. Figure S1. $\%\text{Ca}$ precipitation at $T = 60^\circ\text{C}$ at different CO_3/Ca molar ratio and different Na_2CO_3 addition flowrates vs. the time ($V_{\text{SB}} = 250 \text{ mL}$, $[\text{Na}_2\text{CO}_3] = 1 \text{ M}$). (a) Na_2CO_3 addition flowrate 393.5 and 465.1 $\mu\text{L}/\text{min}$ for CO_3/Ca molar ratio 1.1 ($V_{\text{Na}_2\text{CO}_3, \text{added}} = 5903.15 \mu\text{L}$) and 1.3

($V_{\text{Na}_2\text{CO}_3, \text{added}} = 6976.45 \mu\text{L}$), respectively; (b) same of run (a) but successive Na_2CO_3 addition for a total $V_{\text{Na}_2\text{CO}_3, \text{added}} = 5903.15 \times 2$ and $6976.45 \times 2 \mu\text{L}$. Figure S2. % Ca and %Mg precipitation in presence of antiscalant (2 mg L^{-1}) using different addition mode of the precipitant vs. time ($V_{\text{SB}} = 500 \text{ mL}$; $V_{\text{Na}_2\text{CO}_3, \text{added}} = 18.2 \text{ mL}$, $[\text{Na}_2\text{CO}_3] = 0.65 \text{ M}$, CO_3/Ca ratio = 1.1; CO_3_{33} : syringe pump ($910 \mu\text{L}/\text{min}$); CO_3_{34} : addition to 100 mL of SB and mixing by vortex, then addition to remaining 400 mL and energetic stirring for 5 min; CO_3_{35} : addition to 100 mL of SB and mixing by vortex then addition to remaining 400 mL and sonication for 5 min; $T = 35 \text{ }^\circ\text{C}$). Figure S3: % Ca and %Mg precipitation in presence of minor ions and antiscalant at $T = 15 \text{ }^\circ\text{C}$ ($V_{\text{SB}} = 500 \text{ mL}$, Na_2CO_3 addition: 18.2 mL , 0.65 M , $1.82 \text{ mL}/\text{min}$ for 10 min; CO_3/Ca ratio = 1.1). Figure S4. % Ca and %Mg precipitation in presence of minor ions and antiscalant at $T = 35 \text{ }^\circ\text{C}$. ($V_{\text{SB}} = 500 \text{ mL}$, Na_2CO_3 addition: 18.2 mL , 0.65 M , $1.82 \text{ mL}/\text{min}$ for 10 min; CO_3/Ca ratio = 1.1). Figure S5. Flowchart showing the Ca reduction from RO-brine. Table S3. Life cycle impact assessment (LCIA) results of the near-ambient temperature calcium precipitation process. Calculated with Environmental Footprint 3.0 method (EF 3.0, adapted for SimaPro), using SimaPro LCA software.

Author Contributions: R.M.: Conceptualization, Methodology, Writing—original draft, Writing—review and editing, Supervision. A.H.A.: Investigation, Methodology. E.C.: Review, Visualization. D.S.D.: Ex ante LCA assessment, Methodology, Writing. C.V.G.: Ex ante LCA assessment. J.J.E.G.: Ex ante LCA assessment. P.A.: Investigation, Methodology, Writing—review and editing. All authors have read and agreed to the published version of the manuscript.

Funding: This research was funded by European Union grant number (ID 869703).

Data Availability Statement: The original contributions presented in the study are included in the article and supplementary material, further inquiries can be directed to the corresponding author.

Acknowledgments: We would like to thank Daniel E. Gerard (Omya International AG) for some general discussions with R.M. on possible design configurations of crystallizers for calcium precipitation. We would like to thank Jose Luis Cortina (UPC—Universidad Politecnica de Catalunya) for the SEM micrographs and EDS analyses on the CaCO_3 precipitates. The financial support of the European Union for the H2020-SC5-2019-2 SEA4VALUE project (<https://sea4value.eu/>, accessed on 09 January 2024) under grant agreement ID 869703 is acknowledged.

Conflicts of Interest: The authors declare no conflict of interest.

References

1. Sangeetha, A.; Shanmugan, S.; Alrubaie, A.J.; Jaber, M.M.; Panchal, H.; Attia, M.E.H.; Elsheikh, A.H.; Mevada, D.; Essa, F.A. A review on PCM and nanofluid for various productivity enhancement methods for double slope solar still: Future challenge and current water issues. *Desalination* **2023**, *551*, 116367. [[CrossRef](#)]
2. Curto, D.; Franzitta, V.; Guercio, A. A review of the water desalination technologies. *Appl. Sci.* **2021**, *11*, 670. [[CrossRef](#)]
3. Shah, K.M.; Billinge, I.H.; Chen, X.; Fan, H.; Huang, Y.; Winton, R.K.; Yip, N.Y. Drivers, challenges, and emerging technologies for desalination of high-salinity brines: A critical review. *Desalination* **2022**, *538*, 115827. [[CrossRef](#)]
4. Mauter, M.S.; Fiske, P.S. Desalination for a circular water economy. *Energy Environ. Sci.* **2020**, *13*, 3180–3184. [[CrossRef](#)]
5. Panagopoulos, A.; Haralambous, K.-J.; Loizidou, M. Desalination brine disposal methods and treatment technologies—A review. *Sci. Total Environ.* **2019**, *693*, 133545. [[CrossRef](#)] [[PubMed](#)]
6. Elsheniti, M.B.; Ibrahim, A.; Elsamni, O.; Elewa, M. Experimental and economic investigation of sweeping gas membrane distillation/pervaporation modules using novel pilot scale device. *Sep. Purif. Technol.* **2023**, *310*, 123165. [[CrossRef](#)]
7. Al-Obaidi, M.; Alsarayreh, A.; Al-Hroub, A.; Alsadaie, S.; Mujtaba, I. Performance analysis of a medium-sized industrial reverse osmosis brackish water desalination plant. *Desalination* **2018**, *443*, 272–284. [[CrossRef](#)]
8. Panagopoulos, A.; Haralambous, K.-J. Minimal Liquid Discharge (MLD) and Zero Liquid Discharge (ZLD) strategies for wastewater management and resource recovery—Analysis, challenges and prospects. *J. Environ. Chem. Eng.* **2020**, *8*, 104418. [[CrossRef](#)]
9. Mero, J.L. The mineral resources of the sea. *Geol. Mag.* **1965**, *102*, 565. [[CrossRef](#)]
10. European Commission, Directorate-General for Internal Market, Industry, Entrepreneurship and SMEs; Blengini, G.; El Latunussa, C.; Eynard, U.; Torres De Matos, C.; Wittmer, D.; Georgitzikis, K.; Pavel, C.; Carrara, S.; Mancini, L.; et al. Study on the EU's List of Critical Raw Materials (2020); final report; Publications Office of the European Union. 2020. Available online: <https://data.europa.eu/doi/10.2873/11619> (accessed on 9 January 2024).
11. Bhandari, M.; Kharkwal, S.; Prajapati, S.K. Recycling drinking water RO reject for microalgae-mediated resource recovery. *Resour. Conserv. Recycl.* **2023**, *188*, 106699. [[CrossRef](#)]

12. Yoon, T.J.; Sharan, P.; Craddock, E.P.; Lewis, J.C.; Matteson, J.A.; Seong, J.G.; Singh, R.P.; Maerzke, K.A.; Currier, R.P.; Findikoglu, A.T. Selective recovery of critical materials in zero-liquid discharge supercritical water desalination. *Desalination* **2022**, *537*, 115849. [[CrossRef](#)]
13. Figueira, M.; Rodríguez-Jiménez, D.; López, J.; Reig, M.; Cortina, J.L.; Valderrama, C. Experimental and economic evaluation of nanofiltration as a pre-treatment for added-value elements recovery from seawater desalination brines. *Desalination* **2023**, *549*, 116321. [[CrossRef](#)]
14. Cucurachi, S.; van der Giesen, C.; Guinée, J. Ex-ante LCA of Emerging Technologies. *Procedia CIRP* **2018**, *69*, 463–468. [[CrossRef](#)]
15. Giwa, A.; Dufour, V.; Al Marzooqi, F.; Al Kaabi, M.; Hasan, S.W. Brine management methods: Recent innovations and current status. *Desalination* **2017**, *407*, 1–23. [[CrossRef](#)]
16. Pérez-González, A.; Ibáñez, R.; Gómez, P.; Urriaga, A.M.; Ortiz, I.; Irabien, J.A. Recovery of desalination brines: Separation of calcium, magnesium and sulfate as a pre-treatment step. *Desalination Water Treat.* **2014**, *56*, 3617–3625. [[CrossRef](#)]
17. Zhao, J.; Wang, M.; Lababidi, H.M.S.; Al-Adwani, H.; Gleason, K.K. A review of heterogeneous nucleation of calcium carbonate and control strategies for scale formation in multi-stage flash (MSF) desalination plants. *Desalination* **2018**, *442*, 75–88. [[CrossRef](#)]
18. Antony, A.; Low, J.H.; Gray, S.; Childress, A.E.; Le-Clech, P.; Leslie, G. Scale formation and control in high pressure membrane water treatment systems: A review. *J. Membr. Sci.* **2011**, *383*, 1–16. [[CrossRef](#)]
19. Cruz, C.; Herrera-León, S.; Calisaya-Azpilcueta, D.; Salazar, R.; Cisternas, L.A.; Kraslawski, A. Using Waste Brine from Desalination Plant as a Source of Industrial Water in Copper Mining Industry. *Minerals* **2022**, *12*, 1162. [[CrossRef](#)]
20. Mahmud, N.; Alvarez, D.V.F.; Ibrahim, M.H.; El-Naas, M.H.; Esposito, D.V. Magnesium recovery from desalination reject brine as pretreatment for membraneless electrolysis. *Desalination* **2021**, *525*, 115489. [[CrossRef](#)]
21. Mahmud, N.; Ibrahim, M.H.; Alvarez, D.V.F.; Esposito, D.V.; El-Naas, M.H. Evaluation of parameters controlling calcium recovery and CO₂ uptake from desalination reject brine: An optimization approach. *J. Clean. Prod.* **2022**, *369*, 133405. [[CrossRef](#)]
22. Casas, S.; Aladjem, C.; Larrotcha, E.; Gibert, O.; Valderrama, C.; Cortina, J.L. Valorisation of Ca and Mg by-products from mining and seawater desalination brines for water treatment applications. *J. Chem. Technol. Biotechnol.* **2014**, *89*, 872–883. [[CrossRef](#)]
23. Wang, Y.; Qin, Y.; Wang, B.; Jin, J.; Wang, B.; Cui, D. Selective removal of calcium ions from seawater or desalination brine using a modified sodium carbonate method. *Desalination Water Treat.* **2020**, *174*, 123–135. [[CrossRef](#)]
24. Molinari, R.; Avci, A.H.; Argurio, P.; Curcio, E.; Meca, S.; Plà-Castellana, M.; Cortina, J.L. Selective precipitation of calcium ion from seawater desalination reverse osmosis brine. *J. Clean. Prod.* **2021**, *328*, 129645. [[CrossRef](#)]
25. Molinari, R.; Avci, A.H.; Argurio, P.; Curcio, E.; Meca, S.; Casas, S.; Plà-Castellana, M.; Arpke, H.; Cortina, J.L. Can Brine from Seawater Desalination Plants Be a Source of Critical Metals? *ChemViews* **2022**. [[CrossRef](#)]
26. Amann, A.; Zoboli, O.; Krampe, J.; Rechberger, H.; Zessner, M.; Egle, L. Environmental impacts of phosphorus recovery from municipal wastewater. *Resour. Conserv. Recycl.* **2018**, *130*, 127–139. [[CrossRef](#)]
27. Arashiro, L.T.; Montero, N.; Ferrer, I.; Acién, F.G.; Gómez, C.; Garfí, M. Life cycle assessment of high rate algal ponds for wastewater treatment and resource recovery. *Sci. Total Environ.* **2018**, *622–623*, 1118–1130. [[CrossRef](#)] [[PubMed](#)]
28. Blue, C.R.; Giuffre, A.; Mergelsberg, S.; Han, N.; De Yoreo, J.J.; Dove, P.M. Chemical and physical controls on the transformation of amorphous calcium carbonate into crystalline CaCO₃ polymorphs. *Geochim. Cosmochim. Acta* **2017**, *196*, 179–196. [[CrossRef](#)]
29. Barlow, D.A.; Baird, J.K.; Su, C.-H. Theory of the von Weimarn rules governing the average size of crystals precipitated from a supersaturated solution. *J. Cryst. Growth* **2004**, *264*, 417–423. [[CrossRef](#)]
30. Wu, D.T. The time lag in nucleation theory. *J. Chem. Phys.* **1992**, *97*, 2644–2650. [[CrossRef](#)]
31. Buyevich, Y.; Mansurov, V.V. Kinetics of the intermediate stage of phase transition in batch crystallization. *J. Cryst. Growth* **1990**, *104*, 861–867. [[CrossRef](#)]
32. Lifshitz, I.; Slyozov, V.V. The kinetics of precipitation from supersaturated solid solutions. *J. Phys. Chem. Solids* **1961**, *19*, 35–50. [[CrossRef](#)]
33. Marqusee, J.A.; Ross, J. Kinetics of phase transitions: Theory of Ostwald ripening. *J. Chem. Phys.* **1983**, *79*, 373–378. [[CrossRef](#)]
34. Marqusee, J.A.; Ross, J. Theory of Ostwald ripening: Competitive growth and its dependence on volume fraction. *J. Chem. Phys.* **1984**, *80*, 536–543. [[CrossRef](#)]
35. Pan, Y.; Li, Y.; Ma, Q.; He, H.; Wang, S.; Sun, Z.; Cai, W.-J.; Dong, B.; Di, Y.; Fu, W.; et al. The role of Mg²⁺ in inhibiting CaCO₃ precipitation from seawater. *Mar. Chem.* **2021**, *237*, 104036. [[CrossRef](#)]
36. Zhang, D.; Lin, Q.; Xue, N.; Zhu, P.; Wang, Z.; Wang, W.; Ji, Q.; Dong, L.; Yan, K.; Wu, J.; et al. The kinetics, thermodynamics and mineral crystallography of CaCO₃ precipitation by dissolved organic matter and salinity. *Sci. Total. Environ.* **2019**, *673*, 546–552. [[CrossRef](#)]
37. Morse, J.W.; Wang, Q.; Tsio, M.Y. Influences of temperature and Mg:Ca ratio on CaCO₃ precipitates from seawater. *Geology* **1997**, *25*, 85–87. [[CrossRef](#)]
38. Kawano, M.; Hwang, J. Roles of microbial acidic polysaccharides in precipitation rate and polymorph of calcium carbonate minerals. *Appl. Clay Sci.* **2011**, *51*, 484–490. [[CrossRef](#)]
39. Zuddas, P.; Pachana, K.; Faivre, D. The influence of dissolved humic acids on the kinetics of calcite precipitation from seawater solutions. *Chem. Geol.* **2003**, *201*, 91–101. [[CrossRef](#)]
40. Hu, Y.-B.; Wolf-Gladrow, D.A.; Dieckmann, G.S.; Völker, C.; Nehrke, G. A laboratory study of ikaite (CaCO₃·6H₂O) precipitation as a function of pH, salinity, temperature and phosphate concentration. *Mar. Chem.* **2014**, *162*, 10–18. [[CrossRef](#)]

41. Tzotzi, C.; Pahiadaki, T.; Yiantsios, S.G.; Karabelas, A.J.; Andritsos, N. A study of CaCO₃ scale formation and inhibition in RO and NF membrane processes. *J. Membr. Sci.* **2007**, *296*, 171–184. [[CrossRef](#)]
42. Oh, H.-J.; Choung, Y.-K.; Lee, S.; Choi, J.-S.; Hwang, T.-M.; Kim, J.H. Scale formation in reverse osmosis desalination: Model development. *Desalination* **2009**, *238*, 333–346. [[CrossRef](#)]
43. Jain, T.; Sanchez, E.; Owens-Bennett, E.; Trussell, R.; Walker, S.; Liu, H. Impacts of antiscalants on the formation of calcium solids: Implication on scaling potential of desalination concentrate. *Environ. Sci. Water Res. Technol.* **2019**, *5*, 1285–1294. [[CrossRef](#)]
44. Istirokhatun, T.; Dewi, M.N.; Ilma, H.I.; Susanto, H. Separation of antiscalants from reverse osmosis concentrates using nanofiltration. *Desalination* **2018**, *429*, 105–110. [[CrossRef](#)]
45. McCool, B.C.; Rahardianto, A.; Cohen, Y. Antiscalant removal in accelerated desupersaturation of RO concentrate via chemically-enhanced seeded precipitation (CESP). *Water Res.* **2012**, *46*, 4261–4271. [[CrossRef](#)] [[PubMed](#)]
46. Kabalnov, A. Thermodynamic and theoretical aspects of emulsions and their stability. *Curr. Opin. Colloid Interface Sci.* **1998**, *3*, 270–275. [[CrossRef](#)]
47. Sharqawy, M.H.; Lienhard, J.H.; Zubair, S.M. Thermophysical properties of seawater: A review of existing correlations and data. *Desalination Water Treat.* **2010**, *16*, 354–380. [[CrossRef](#)]
48. Cambridge, M.L.; Zavala-Perez, A.; Cawthray, G.R.; Mondon, J.; Kendrick, G.A. Effects of high salinity from desalination brine on growth, photosynthesis, water relations and osmolyte concentrations of seagrass *Posidonia australis*. *Mar. Pollut. Bull.* **2017**, *115*, 252–260. [[CrossRef](#)]
49. Missimer, T.M.; Maliva, R.G. Environmental issues in seawater reverse osmosis desalination: Intakes and outfalls. *Desalination* **2018**, *434*, 198–215. [[CrossRef](#)]

Disclaimer/Publisher’s Note: The statements, opinions and data contained in all publications are solely those of the individual author(s) and contributor(s) and not of MDPI and/or the editor(s). MDPI and/or the editor(s) disclaim responsibility for any injury to people or property resulting from any ideas, methods, instructions or products referred to in the content.